Optical peRformanCe monitoring enabling dynamic networks using a Holistic cross-layEr, Self-configurable Truly flexible appRoAch

D2.2 – Impairment monitoring: from a hardware to a software ecosystem

Document Information

Scheduled delivery 01.02.2016

Actual delivery

Version V0_7

Responsible Partner NBLF (ex ALBLF)

Dissemination Level

PU Public

Revision History

Date	Editor	Status	Version	Changes
10.11.2015	NBLF	Draft	ToC	Layout
22.01.2015	NBLF	Draft	V0_1	Added content
26.01.2015	NBLF	Draft	V0_2	Added Content + formatting
27.01.2015	NBLF	Draft	V0_3	Intro
28.01.2015	NBLF	Draft	V0_4	First revision
28.01.2016	SSSA	Draft	V0_41	Review
29.01.2015	NBLF	Draft	V0_5	Corrections
29.01.2015	NBLF	Draft	V0_6	Section 2 “Faster return of investment in WDM networks when elastic networks dynamically fit ageing of link margins” removed upon agreement amongst partners
31.01.2016	CTI	Draft	V0_61	Review
01.02-2016	NBLF	Final	Final	Final version.

Contributors

Camille Delezoide (NBLF), Yvan Pointurier (NBLF), Jelena Pesic (NBLF), Fabien Boitier (NBLF), Petros Ramantanis (NBLF), Thierry Zami (Nokia France), Annalisa Morea (Nokia Italy), Sébastien Bigo (NBLF)

Stefanos Dris (NTUA), Nikos Argyris (NTUA)

Andrea Di Giglio (TILAB), Annachiara Pagano (TILAB), Diego Roccato (TILAB)

Internal Reviewers

CTI, SSSA

Copyright

Acknowledgements

The research leading to these results has received funding from the EC HORIZON 2020 under grant agreement n° 645360.

Glossary of Acronyms

Acronym	Definition
ABNO	Application-Based Network Operations
ADC	Analog-to-Digital Converter
API	Application Programming Interfaces
ASE	Amplified Spontaneous Emission
ASIC	Application-Specific Integrated Circuit
AWG	Array waveguide grating
BER	Bit Error Rate
BOL	Beginning of Life
BVT	Bandwidth Variable Transponder
CAPEX	Capital Expenditure
CCAMP-WG	Common Control and Measurement Plane Working Group
CD	Chromatic Dispersion
C&M	Control and Monitoring
CMA	Constant Modulus Algorithm
CPR	Carrier phase recovery
D	Deliverable
DCM	Dispersion compensating Module
DGD	Differential Group Dispersion
DLI	Delay line interferometer
DoW	Description of Work
DSLAM	Digital Subscriber Line Access Multiplexer
DSP	Digital Signal Processor
EC	European Commission
EDFA	Erbium doped Fibre Amplifier
EOL	End of Life

FEC	Forward error correction
FOE	Frequency Offset Estimator
FTTC	Fibre to the Cabinet
FWM	Four Wave Mixing
GMPLS	Generalised Multi Protocol Label Switching
GN	Gaussian Noise model
GSM	Global System for Mobile Communications
ICT	Information and Communication Technologies
LSP-DB	Label Switched Path DataBase
LTE	Long-Term Evolution
L-UFL	Local unambiguous failure localization
LO	Local oscillator
M	Milestone
MFVT	Modulation Format Variable Transponders
NLI	Non Linear Interference
MMSE	Minimum Mean Squared Error
NMS	Network Management System
MIMO	Multiple Input and Multiple Output
MPI	Multi Path Interference
NMS	Network Management System
NXW	Nextworks
OAM	Operations, Administration, and Maintenance
OCh	Optical channel
OCM	Optical Channel Monitoring
ODU	Optical Data Unit
OLO	Other Licensed Operators
OLT	Optical Line Terminal
OPEX	Operational Expenditure
OPB	Optical packet backbone

OPM	Optical Performance Monitoring
OSA	Optical Spectrum Analyser
OSNR	Optical Signal to Noise Ratio
OSPF-TE	Open Shortest Path First – Traffic Engineering
OTN	Optical Transport Network
OXC	Optical cross Connect
PCE	Path Computation Element
PDL	Polarization Dependent Loss
PDM	Polarization Division Multiplexing
PM	Project Manager
PM-*m*QAM	Polarization multiplexing *m* quadrature amplitude modulation
PM-QPSK	Polarization multiplexing quadrature phase shift keying
PMD	Polarization Mode Dispersion
PO	Project Officer
PON	Passive Optical Network
POP	Point of Presence
PSP	Principal States of Polarization
PT	Packet Transport
PPM	Protocol Performance Monitoring
PU	Public
QAM	Quadrature amplitude modulation
QoS	Quality of Service
QoT	Quality of Traffic
QPSK	Quadrature phase shift keying
RMSPA	Routing, Modulation, Spectrum, and Power Assignment
ROADM	Reconfigurable Optical Add/Drop Multiplexer
RF	Radio Frequency
RX	Receiver
SD-FEC	Soft Decision Forward Error Correction

SMF	Single Mode Fibre
RWA	Routing and Wavelength Assignment
SDH	Synchronous Digital Hierarchy
SDN	Software Defined Networking
SLA	Service-level agreement
SNR	Signal to Noise Ratio
Soft-OPM	Software-based OPM
SOP	State of Polarization
SPM	Self Phase Modulation
SSS	Spectrum Selective Switch
SSSA	Scuola Superiore Sant'Anna
TED	Traffic Engineering Database
TILAB	Telecom Italia Lab
TRX	Transponder
Tx	Transmitter
UMTS	Universal Mobile Telecommunications System
WDM	Wavelength Division Multiplexing
WSON	Wavelength Switched Optical Network
WSS	Wavelength Selective Switch
WP	Work Package
XPM	Cross Phase Modulation

Table of Contents

Executive summary

Relying on literature reviews and laboratory experiments, this deliverable specifies which physical layer parameters are of the utmost importance to monitor in present and future optical networks. This deliverable also presents existing technical solutions to monitor parameters of interest using software solutions, thus leveraging the monitoring capacities of coherent transponders towards dynamic networks.

Introduction

In this deliverable, relying on the most recent literature and the technical state of the art, we provide examples of parameters that are likely to make a difference if monitored and used at the scale of the network. Moreover we provide rational methods that can be used to determine which parameters should be monitored, and eventually assess the benefits such monitoring could bring.

A short literature review on software-based optical performance monitoring (soft-OPM) is enough to demonstrate the huge amount of parameters that could be monitored using state-of-the-art coherent transponders integrating an extra software layer. This layer would be dedicated to recycle data from the coherent demodulation process to turn the coherent transponder into a multi-purpose measuring instrument.

It is highly probable that with enough development, any physical layer parameter could be measured with sufficient accuracy to be thought as reliable information, in the context of dynamic networks, for network optimization.

Accordingly, how to measure a parameter is not as topical a question as which parameter to monitor. When the first question can be considered as a purely technical issue, the second can be thought of as far more complicated to answer. Indeed, knowing which parameter to monitor requires to imagine at the scale of an entire optical network how this extra information can be used for optimization purposes, then to figure out if the scheme involved would bring sufficient benefits to be adopted by the industry.

In Section 1, we review margins used in optical networks and show how they can be reduced through proper design to increase network capacity. In this study, flexible optoelectronic nodes coupled with optical monitoring appear as keys to fully leverage network margins. Also, the study shows how physical parameters that play a major role in the performance of a link could be monitored during training phases in order to reduce design margins in network update scenarios.

From section 1, we build a better understanding on how the monitoring of parameters that impact performance can leverage benefits. In Section 2, we thus explore all possible effects and associated physical parameters that may impact performance in a coherent optical network. In the same approach, we focus on Section 3 on filtering effects which are expected to have the most impact in future optical networks as bandwidth occupancy reaches its limits. We experimentally study how filtering effects from Reconfigurable Optical Add/Drop Multiplexer (ROADM) nodes may impact the performance of the transmission, and therefore underline the importance of monitoring the equivalent filter cascade of a link. In particular we show that, in metro networks, optimal pulse shaping should not be solely

driven by bandwidth reduction and spectral efficiency as in long-haul networks. Then, in Section 4, we provide a state of the art review of published monitoring algorithms that could be employed for the purposes of ORCHESTRA project, followed by an experimental assessment of some of these algorithms in Section 5.

Finally, in Section 6, we conclude with a restricted list of parameters that seem to be the most suited to monitor and utilization in the context of ORCHESTRA.

1. Design of low-margin optical networks

The work presented in this section led to publication [1].

1.1. Margins in optical transport networks

Significant margins are considered as mandatory to ensure that an optical network supports the planned demand capacity during network deployment or when deploying a new service (a lightpath) virtually error-free during operation over the full network life, which may span several decades. At the optical layer, the margin of a lightpath may be quantified as the difference between the actual quality of transmission (QoT) metric (e.g., electrical or optical signal to noise ratio (SNR/OSNR), Q^2-factor, reach, bit error rate) of the signal supporting the lightpath, and the threshold above which the signal is deemed recoverable error-free (i.e., the Forward Error Correction (FEC) limit). In [2], Augé proposed the following margins taxonomy: system margins (thereafter, S-margins), unallocated margins (U-margins), and design margins (D-margins).

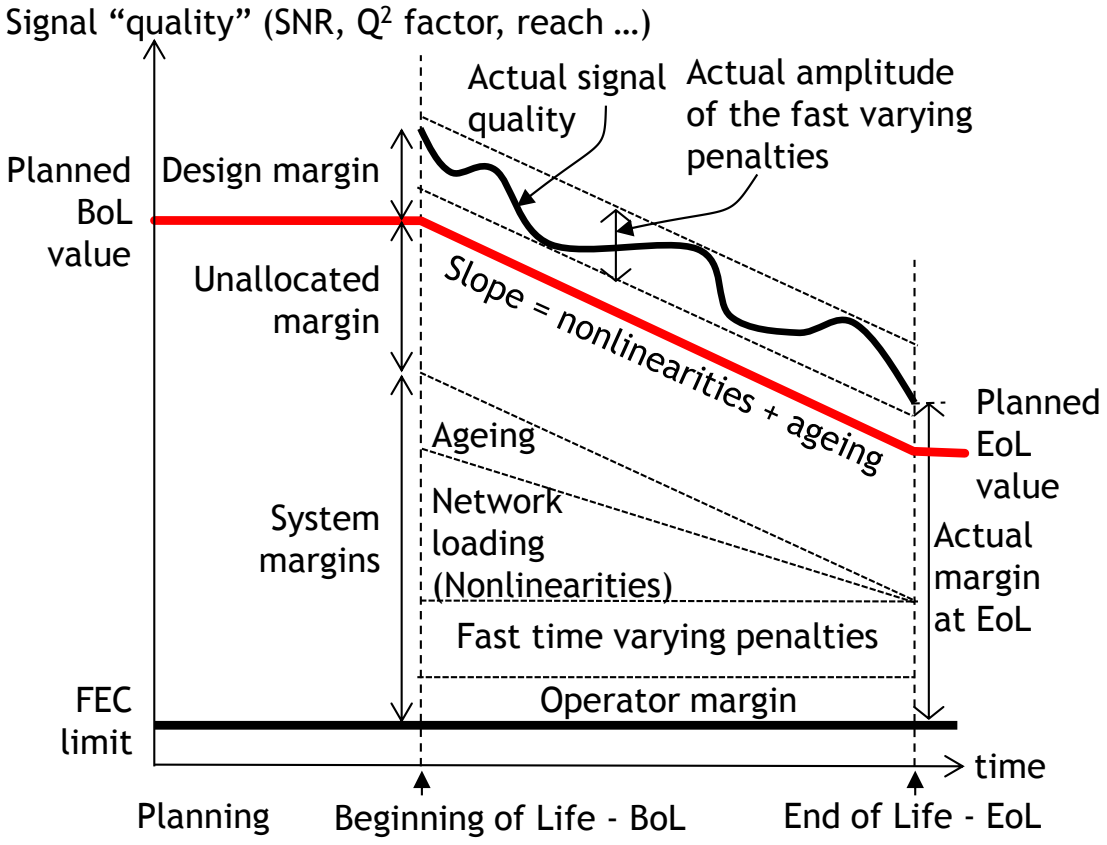

Figure 1-1: Margins and their evolution in a transport optical network.

In the following, we first review the margins types, their key characteristics and their typical values. We then explain how each type of margin can be reduced through careful network planning, using a combination of flexible equipment (transponders – TRX –, optical and electronic switching fabrics) for the U- and S-margins, and monitoring for the D-margins. Last, we outline the upcoming challenges to design and operate a low-margin network.

S-margins account for time-varying network operating conditions. S-margins include fast varying impairments such as polarization effects, and slow varying impairments; the latter are due to either increasing channel loading during the network life, which translates into additional nonlinearities, or to network equipment ageing: increasing fibre losses due to splices to repair fibre cuts, degrading amplifier noise factor, and detuning of the lasers leading to misalignment with optical filters in the intermediate nodes. S-margins may include an additional operator margin [2]. S-margins define the minimum quality value of the signal to be met at network Beginning of Life (BoL).

U-margins encompass both the capacity and reach margins, i.e., the difference of capacity/reach between the demand and that of the equipment, in particular the TRX that are really deployed. U-margins result from the discrete datarate and reach granularity of commercial transmission equipment.

D-margins are the difference between the planned BoL value and the real value of the quality metric, and are due to the inaccuracy of the design tool used to evaluate the QoT of all signals during network planning, which stem from two main sources: the inaccuracy of the inputs of the QoT model, and the inaccuracy of the QoT model itself. Margin evolution with time is illustrated in Figure 1-1 and typical values can be found in Table 1-1. As an example, consider a 600 km long lightpath carrying a 100G PDM-QPSK signal with soft decision FEC active for 10 years in a network with route-and-select optical crossconnects (i.e., 2 filters per intermediate node), 100 km fibre spans of standard single mode fibre with no in-line dispersion compensation, 1 node every 100 km, and amplifier noise factor of 4.5 dB. Assuming 2 dB (SNR) margins for the nonlinearities, the S-margins are 4.7 dB. At BoL, assuming a completely unloaded system and using the model in [3], and accounting for penalties of 1 dB for TRX and 0.03 dB per filter, the reach of such a system is ~7100 km resulting in a combined U- and S-margins of 10.7 dB, i.e. U-margins of 6 dB. We assume D-margins of 1 dB, resulting in an 11.7 dB SNR margin at BoL. Assuming that components have aged as planned (typically a worst case) and that the network is fully loaded, the S-margins ideally amount to 0.4 dB (i.e., fast varying effects) at network End of Life (EoL), for a total EoL margin of 7.4 dB.

Table 1-1: Margin types and typical values

Margin type	**SNR Margin**	**Margin type**	**SNR margin**
Unallocated margins (U)	Several dB	Fibre ageing (cuts) (S)	1.6e-3 dB/km/year (OSNR) [6]
Design margins (D)	<2 dB [2]	Nodes ageing (filtering) (S)	0.05 dB / filter [7], [8]
Nonlinearities (S)	1.5-3dB [4]	Transponder ageing (S)	0.5 dB [8]
Amplifier NF ageing (S)	0.7 dB [5]	Fast variations (S)	0.4 dB [9]

1.2. Flexible equipment for unallocated and system margin reduction

As explained in [2], U-margins are not known until the network is deployed, and thus can only be leveraged after deployment or on network upgrades. U-margins may be partially or even completely used through the utilization of a rate-flexible transponder (flex-TRX), which adjusts its datarate to the targeted reach. Coarse granularity flex-TRX (e.g., 100/200/400G) will use only part of the U-margins, while fine granularity flex-TRX (leveraging for instance time hybrid QAM or 4-D modulation formats) [10],[11],[12] may use all of it.

S-margins are also known after network deployment, and may vary with time. Fast time varying effects, such as fast SOP variations, that are not directly mitigated through TRX digital signal processing may be translated into capacity only at the expense of reduced network resilience, or to time-varying transported capacity which may temporarily be below the demand.

Slow varying effects such as nonlinear effects, which increase as new channels are lit, and component ageing, are more predictable, and may be leveraged when upgrading the network. To fully leverage S-margins stemming from network loading (i.e., from nonlinear impairments), careful power allocation is required; in fact, each lightpath may have its own modulation and power, leading to a RMSPA (routing, modulation, spectrum, power allocation) network design problem. At the lightpath level, [13] shows that, when accounting for the exact link load, the reach for a standard PDM-QPSK signal is almost double at BoL compared with EoL (see also D4.1); the highest reach gains are achieved in lightly loaded networks when nonlinearities are smaller, i.e., in the early stages of the life of the network. At the network level, the supported traffic capacity increase through leveraging the (nonlinear) S-margins yields a capacity gain of ~30% for a continental network, while the joint exploitation of the U- and S-margins (nonlinear effects only) reaches 60% [4]. Authors in [14] find similar results for continental networks.

Furthermore, margin reduction through equipment data rate variation enables to use costly equipment at maximum capacity upon network deployment, and to delay investments to later stages of the network life to benefit from equipment cost erosion [15]. The impact of such multi-year network planning is further studied in [8], where slow variations only account for ageing (typically 2 dB in a national network).

1.3. Monitoring for design margin reduction

D-margins come from the uncertainty of both the QoT estimation tool, and of the inputs of the tool, which include topological information (link attenuation, chromatic dispersion map …) and network equipment characteristics (amplifier noise factor, filter alignment …).Those two effects are fundamentally difficult to separate and their compounded impact is only known at deployment time. It is, however, possible to reduce the QoT tool inputs uncertainty through monitoring techniques, in order to make more accurate QoT prediction for new lightpaths during network upgrades. Consider the 2-step process illustrated in Figure 1-2. A resource allocation tool (e.g., RMSPA) is used at network planning time, with imperfect knowledge of the topology $G+\varepsilon_G$ (where G abstracts the actual physical topology e.g. link lengths, dispersion map,… and ε_G quantifies the uncertainty on G) and imperfect knowledge of the deployed equipment characteristics $E+\varepsilon_E$ subject to traffic demand D. Uncertainties are accounted for a resource allocation algorithm via D-margins $m=f(\varepsilon_G,\varepsilon_E)$; these margins can be pre-defined or dependent on each lightpath, e.g. longer lightpaths may be associated with higher margin as in [16].

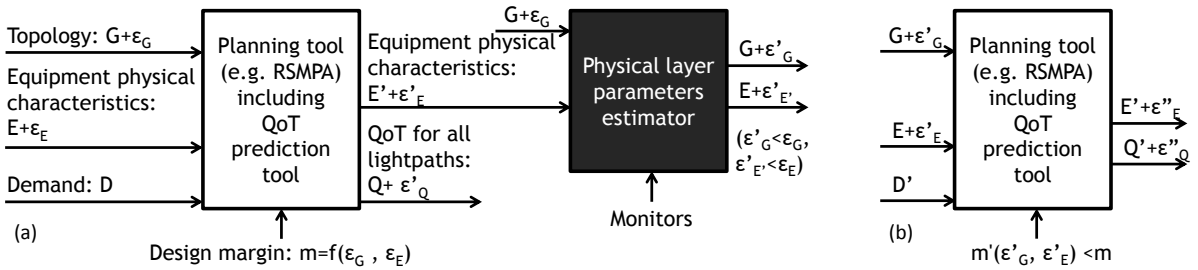

Figure 1-2: Design margins reduction with monitoring. (a) Training phase; (b) Estimation phase.

After the network is deployed, D-margins are known and may be mitigated with flexible equipment as with the U- and S-margins, however, any new lightpath will still be subject to the original D-margins. To avoid this, it is possible to leverage the wealth of path-level monitoring information made available by coherent receivers almost for free, including received power, residual chromatic dispersion, noise level, and polarization [17]. This additional information can be used to feed a "physical layer parameters estimator", which

goal is to refine the knowledge of the underlying physical layer (Figure 1-2a) and thus decrease (ε_G, ε_E) to (ε'_G,ε'_E). The network planner will then be able to use lower D-margins $m'(\varepsilon'_G,\varepsilon'_E)$ when establishing a new lightpath upon a network upgrade (Figure 1-2b). Observe that QoT estimators typically require link-level characteristics while coherent receivers yield path-level measurements; link-level metrics may be obtained via correlation techniques such as network kriging [18] when the characteristics are linearly additive (i.e. addition of link-level metrics yields path-level metric), or more advanced techniques such as machine learning, which are better adapted to nonlinear network characteristics [19]. Suitable correlation techniques are described further in depth in WP4, and more specifically in D4.1.

1.4. Challenges

Although designing low-margin networks can result in a clear network capacity increase (60%, not accounting for the D-margins [4]), translation into CAPEX gains will prove challenging for the following reasons. First, margins are highly fragmented, despite the total margin reaching an appealing 10 dB or even more, as mentioned in the example above. The U-margins (several dB) are easier to leverage, essentially requiring flexible transponders. Within the S-margins, the fast variable component (a fraction of a dB) will be difficult to leverage, as either a fast variable transponder, or a fast reconfigurable network infrastructure, would be needed. Ageing excluding nonlinearities may reach 3-4 dB, which can only be exploited with proper monitoring. Network loading (nonlinearities) may amount to another 3 dB, but exploiting them requires fine, difficult per-wavelength power tuning. Sophisticated spectrum allocation (adjusting the spectrum guard band between light paths crossing the same fibre) may also help. Mitigating D-margins, which account for less than 2 dB, requires advanced monitoring and control plane support for information correlation [20].

Hence, a flexible network infrastructure is required to fully exploit most margins. Deploying flexible interfaces and varying their capacity with time, however, means that the interfaces' client and WDM sides should be independent. Indeed, demands (on the client side) should be met even when the interface WDM rate changes to adjust to a varying margin. Multilayer nodes that are able to dynamically map electronic resources to optical resources are thus needed. Electronic switching, in addition to the optical transmission equipment, should therefore be provisioned appropriately. This calls for multilayer (electronic and optical), multi-year (accounting for foreseeable ageing such as nonlinearities) routing, spectrum, modulation format, power allocation algorithms relying on monitoring information to constantly adjust network capacity and capacity prediction to the true network state.

1.5. Conclusions

Network margins, although plentiful, require a variety of technologies to be fully exploited and translated into additional capacity: flexible reconfigurable equipment, multilayer electrical/optical nodes and transponders, monitoring, multi-year dimensioning algorithms that can adjust the power of each lightpath and (scalable) support from the control plane. ORCHESTRA extends the state of the art in several of these technologies, targeting to bring solutions that enable margin reductions closer to the market.

2. Coherent transmission systems and fibre transmission impairments

Coherent optical communication is a key enabling technique to satisfy the high data rate requirements in future core networks. Thanks to high-speed electronic devices, coherent detection can now be implemented at very high bit rates, enabling the use of digital signal processing (DSP) techniques against the impairments that the signal undergoes through its physical propagation in fibre and other optical devices. Coherent TRX, nevertheless, introduce their own impairments, which are described in Section 2.1.

Transmission impairments can be categorized into two classes: linear and nonlinear. The major linear impairments (Section 2.2) are chromatic dispersion (CD), polarization mode dispersion (PMD), and polarization dependent loss (PDL). Besides, additional transmission degradations effects should be taken into account, such as power equalization errors that cause optical signal-to-noise ratio (OSNR) unbalancing between OCh in a DWDM comb, and cumulative filtering effects due to flexgrid ROADM. All nonlinear effects (Section 2.3) are described by the Nonlinear Schrödinger Equation (or the Manakov Equation taking into account polarization) through the parameter γ, i.e. the ratio between the silica Kerr nonlinear refractive index n_2 and the fibre effective area A_{eff}. Although they are traditionally described as self phase modulation (SPM), cross phase modulation (XPM), four wave mixing (FWM) etc., they are deeply interconnected and ultimately they can be considered different manifestations of the Kerr effect.

We depict a typical transmission line with no dispersion compensation in Figure 2-1. Signals travel from transmitter to receiver (where the signal beats with the light from a local oscillator for coherent intradyne reception) after traveling over optical fibre, amplifiers, and crossing optical switches.

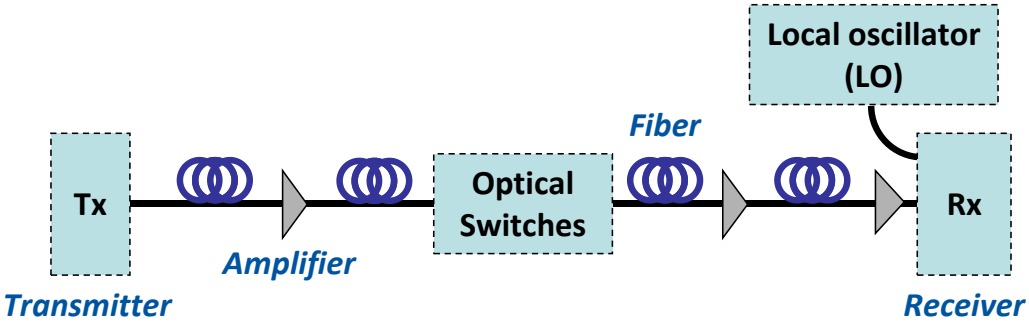

Figure 2-1: Transmission system with no dispersion compensation.

2.1. Impairments from coherent transponders

2.1.1. Frequency mismatch between Tx and LO lasers

In coherent intradyne systems the transmitter (Tx) and local oscillator (LO) lasers are neither frequency-, nor phase-locked to each other. As a consequence, there will always be a slight offset in the emission frequencies of the two lasers, which manifests itself as a proportional rotation of the constellation at the output of the coherent receiver (i.e. after opto-electrical down conversion to the baseband). Large frequency offsets (f_{off}) are also undesirable since they result in a baseband signal that is shifted and no longer centred on zero, leading to spectral distortion through the low pass response of the analogue front end. Frequency accuracy of commercial temperature-stabilized ECL and DFB lasers can typically be ±1-2 GHz, while time stability is of the order of ±0.2 GHz over 12 hours [21] . From the point of view of the receiver DSP, the frequency drift is extremely slow compared to other effects, and can therefore be considered constant over the demodulation process. In general, the more useful measure is the frequency offset × symbol period product ($f_{off}T_s$), since the adverse effects are inversely proportional to the symbol rate of the system.

Let $x[n] = I[n] + jQ[n]$ denote a transmitted sequence of complex M-QAM symbols, over a single polarization. After transmission and coherent reception, the symbols are corrupted by complex AWGN noise, $g[n]$, phase noise due to the combined linewidths of the Tx and LO lasers, $\varphi[n]$, as well as frequency offset, f_{off}. Following ideal symbol clock recovery and equalization in DSP, the received noisy sequence at times $t = nT_s$ (integer n) is given by:

$$\boldsymbol{y[n]} = (\boldsymbol{x[n]} + \boldsymbol{g[n]})\boldsymbol{e^{j(2\pi f_{off} nT_s + \varphi[n])}} \qquad (1)$$

Ignoring phase noise, it is easy to see that a constant f_{off} results in a constant rotation of the noisy received symbols.

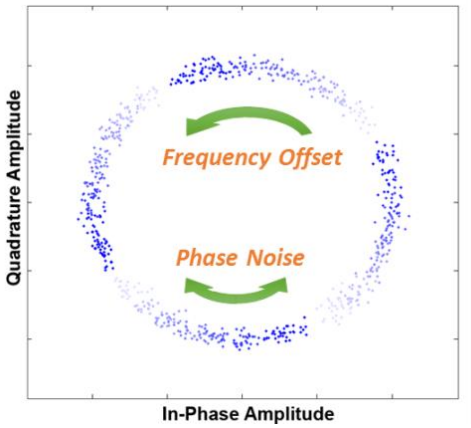

Figure 2-2: Illustrating effects of laser frequency offset and phase noise in a QPSK intradyne system

As long as f_{off} is much smaller than the symbol rate, the rotation of the constellation is easily estimated, tracked and reversed by the receiver DSP. For QPSK, simple phase-increment [22] frequency offset estimation (FOE) schemes suffice, since the modulation can be easily removed using the Viterbi-Viterbi 4^{th} power technique, and the carrier can be isolated. For higher order constellations, more complicated schemes are needed (e.g. [23], [24]). After initial estimation, the offset can be tracked over time by any of the algorithms used for mitigation of linewidth-induced phase noise (see next section). Finally, amplitude noise in *I* and *Q* components of the received signal translate to additional phase noise that adversely affects the estimation accuracy of all algorithms. Appropriate filtering of the estimate is therefore necessary.

2.1.2. Phase noise from Tx and LO lasers

A single-frequency laser is not perfectly monochromatic, exhibiting a certain amount of phase noise and leading to a finite linewidth of the laser output. Like frequency offset, this causes phase variations from symbol to symbol in the received constellation of an intradyne receiver, with the difference that successive offsets in this case are random and rapidly varying. The phase noise due to the combined linewidths of both the Tx and Rx lasers can be described by a random walk where the phase difference between any two observations in the received signal follows a Gaussian distribution, the variance of which is proportional to the time between the observations. Laser phase noise is therefore modelled as a Wiener process with a variance given by:

$$\sigma^2 = 2\pi\Delta\nu T \qquad (2)$$

Where T is the time between observations and $\Delta\nu$ is the 3 dB optical linewidth. Since the effect of phase noise is inversely proportional to the symbol rate, laser linewidth is more often expressed in normalized form in terms of linewidth × symbol period product ($\Delta\nu T_s$). Typical linewidths of commercial lasers is in the MHz-range for DFBs and KHz-range for ECLs. Normalized to the symbol rates of state of the art commercial transceivers (28-32 Gbaud), this leads to values of $\Delta\nu T_s \approx 10^{-6}$ to 10^{-5}.

Carrier phase recovery (CPR) algorithms are straightforward to implement for QPSK; the Viterbi-Viterbi Fourth Power estimator (VV4E) [25] provides an effective means of modulation stripping, after which the phase can be accurately tracked. For 16-QAM and beyond, however, removing the modulation with the VV4E is not possible, since not all symbols lie on equidistant phase axes (90°), as is the case with QPSK. Current schemes therefore rely on alternative methods such as QPSK partitioning [26], the nonlinear least squares (NLS) method [27], or the computationally intensive Blind Phase Search (BPS) algorithm [28]. The best schemes achieve linewidth tolerances of ~10^{-4} for 16-QAM, leaving sufficient operating margin given the linewidths of commercial lasers.

2.1.3. Specific transmitter-side impairments

- **I/Q Gain Imbalance**

I/Q gain imbalance is due to a non-optimal setting of the powers of I and Q RF drive signals. A direct consequence is a disparity of SNR between I and Q signals. I/Q gain imbalance is characterized by a rectangular constellation.

- **I/Q Modulator Bias Error**

I/Q modulator bias errors are due to a non-optimal setting of I, Q or both modulator biases. This error tends to close the eye diagram of the related signal, implying reduced quality of transmission.

- **I/Q Quadrature Error**

I/Q quadrature error happens when the recombination phase for the quadrature signal is not exactly 90°. This results in I/Q crosstalk. I/Q quadrature error is characterized by a rhombic constellation and multiple rails and I and Q eye diagrams.

- **Deterministic Data-Dependent Jitter**

Deterministic data-dependent jitter is due to a deterministic jitter contained in I and Q RF drive signals, originating from the driver circuits. It creates a deterministic opening of the centre of the constellation.

- **Random Data Clock Jitter**

Random data clock jitter occurs when RF drive signals contain a random clock jitter, for example from the VCO reference. The timing jitter cannot be observed in the constellation. Jitter beyond the clock recovery bandwidth will close the decision area in the time domain.

- **Dual-Polarization crosstalk**

Dual-polarization crosstalk at transmitter output can occur when polarization multiplexing is not optimal. This crosstalk is characterized in the constellation diagram by the presence of pseudo-symbols.

- **I/Q Data Skew**

I/Q data skew occurs when the delay D1 between I and Q drive signals is not optimal. It results in an opening of the centre of the constellation.

2.2. Linear propagation effects

2.2.1. Attenuation / Received Optical Power

Received optical power is a crucial parameter in direct detection single span optical system where receiver sensitivity is a function of the span length. In multi-span optical systems, where chains of optical amplifiers are employed, received optical power is usually kept constant by preamplifier optical output power control loop, while noise accumulation is the function that is directly related to span attenuation increase.

Moreover, in an optical system with coherent detection, another element has to be taken into account: information bits are coded in amplitude and phase over two polarisation modes and the received optical power is an overage of data encoded in those four dimensions. For each of them a received optical power value should be specified and this can only be done after beating with the local oscillator; so the received optical power is the amount of signal that effectively beats with the receiver.

On the contrary, some more sophisticated monitoring systems can provide the power of the beating with the local oscillator for each carrier (LSIOPCUR power); the measurement results in Fig refer to a four WDM carriers super-channel in a flexgrid configuration.

It can be seen that Q factor as a function of this value is almost constant. If OSNR is kept constant, independently from the number of carriers, overall power could increase but carrier beating signal (LSIOPCUR) is the key parameter that is related to Q factor.

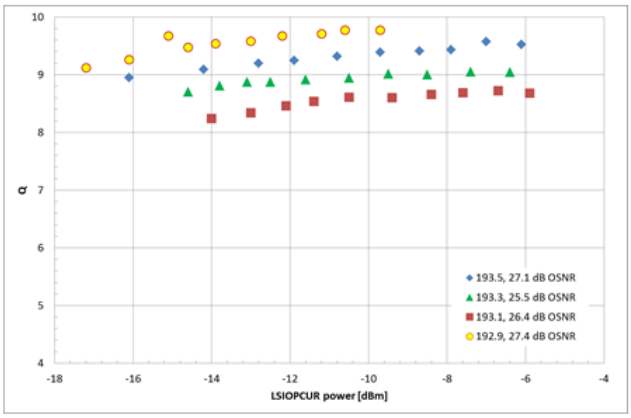

Figure 2-3: Q factor as a function of carrier optical power estimated from electric signal after LO

2.2.2. ASE

Amplified Spontaneous Emission (ASE) is the main source of noise in EDFA amplifiers; noise cumulates along a chain of amplifiers, in an end-to-end optical link. ASE is usually not measured by monitoring systems, since what is important for the QoT is the OSNR value. OSNR itself is not measured in present commercial DWDM systems, but rather estimated from amplifier parameters (G, NF) and measured span attenuations.

A general expression for the final OSNR at the receiver, as a function of the different $OSNR_i$ of the single amplification spans, is:

$$OSNR \approx \left(\sum_{i=1}^{N_s} \frac{1}{OSNR_i} \right)^{-1}, G_i + 1 \approx G_i$$

What is measured at the DSP is usually the error vector magnitude (EVM). This parameter includes also other types of distortions, like crosstalk and nonlinear impairments, in addition to cumulated optical noise.

2.2.3. Back-reflections

Reflectance or optical return loss (which has also been called "back reflection") of a connection is the amount of light that is reflected back up the fibre toward the source by light reflections off the interface of the polished end surface of the mated connectors and air. It is also called Fresnel reflection and is caused by the light going through the change in index of refraction at the interface between the fibre (*n*~1.5) and air (*n*~1). Reflectance is primarily a problem with connectors but may also affect splices. Properly made fusion

splices will have no reflectance; a reflectance peak indicates incomplete fusion or inclusion of an air bubble or other impurity in the splice. The amount of light reflected is determined by the differences in the index of refraction of the two fibres joined, a function of the composition of the glass in the fibre, or any air in the gap between the fibres.

Reflectance in a fibre is measured with an optical time domain reflectometer (OTDR). The OTDR measures the amount of light that's returned from both backscatter in the fibre and reflected from a connector or splice.

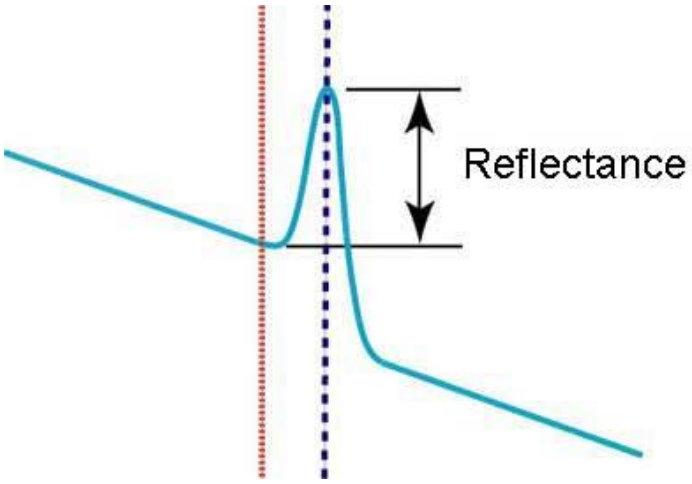

Figure 2-4: Reflectance Peak in an OTDR measurement

In an OTDR, the peak that identifies a reflective event is measured and reflectance calculated. Higher peaks indicate higher reflectance. Reflectance is defined by the amount of light reflected compared to the power of the light being transmitted down the fibre. Thus a 1% reflectance is -20dB, which is about what you get from a flat polished air gap connection, and 1 part per million would be -60dB, typical of an APC connector. Return loss is the opposite, the amount of loss at the level of the return signal, so -20dB reflectance is 20dB return loss.

Table 2-1: Typical reflectances according to connector type

Connector Type	Typical Reflectance
Flat with air gap	-20 dB
Physical Contact (PC)	-30 to -40 dB
Ultra PC	-40 to -50 dB
APC (angled)	-60 dB or higher

Reflectance is one component of the connector's loss, representing about 0.3dB loss for a non-contact or air-gap connector where the two fibres do not make contact. Furthermore, reflectance is sensitive to polarization effects. Carrier networks are often comprised of various types and vintages of optical fibre and splices between cable sections. Older embedded fibre may have mechanical splices that exhibit high reflections, and/or it may have higher transmission loss, in which case the use of distributed Raman amplification may be utilized to bridge long spans [29]. Multiple reflections along a transmission link or double Rayleigh scattering within a fibre amplifier cause time-delayed replicas of the signal to occur. These delayed signals beat with the signal at the receiver and cause the impairment known as multipath interference (MPI). Multipath interference penalty occurs as result of cascaded patch cord with connectors having finite reflection. Each patch cord resembles a Fabry-Perot Etalon and cascaded patch cords acts as an external cavity. Each patch cord may go through destructive or constructive interference as result of temperature, pressure, movements, polarization. A simple approximation to calculated multipath interference is provided by D. Duff [30] where it assumes reflections from more than two patch-cords are negligible.

$$P_{mpi} = 10 \cdot \log_{10}\left[1 - 4N \cdot \sqrt{R_1 \cdot R_2}\right](dB)$$

where N is the number of patch cords cascaded, R_1 and R_2 are reflection at each end of patch cord. For coherent, dual polarization signals, MPI-induced penalties are practically polarization independent, because the PM-QPSK signal is essentially polarization scrambled. At 3.8×10^{-3} BER, approximately 1dB of OSNR penalty was observed for −16 dBc of MPI, whereas a typical MSA transceiver tolerates −15 dBc of MPI with 1 dB of OSNR penalty at 1.9×10^{-2} BER count. The SD-FEC threshold remained at the same pre-FEC BER for MPI as high as −10 dBc, thus indicating that noise from MPI is not degrading the SD-FEC performance.

MPI occurs when the optical signal is multiply reflected within transmission fibre. Distributed Raman amplification can significantly increase the amount of MPI in a system. Crosstalk in photonic devices can cause similar in-band, incoherent crosstalk.

The MPI is primarily attributed to double-Rayleigh scattering along the length of the transmission fibre. The level of MPI becomes intolerable if reflections (such as Rayleigh backscattering or discrete reflections) lie in the region of amplifier. This is because the MPI components are amplified multiply with the gain of amplifier. Double Rayleigh scattering, which is inherently generated within the transmission fibre, would induce a large amount of MPI with a high Raman gain: this MPI imposes a fundamental limitation on Raman amplified systems' performance [31], [32]. Recently, there have also been some efforts to investigate the combined effect of MPI with ASE noise [33] or relative-intensity noise (RIN) of pump laser [34]. Especially, in fibre Raman amplifiers, pump-intensity noise could be transferred to

signal, which, in turn, causes a pump-to-signal crosstalk [35]. In order to suppress the effect of this crosstalk, counter-pumped configurations have been widely used in Raman amplified systems. This is because the different direction of signal and pump propagation could average the impact of pump-to-signal crosstalk in counter-pumped configurations. However, it has been reported that the MPI would be enhanced by the pump-intensity noise in a counter-pumped Raman amplifier [34]. In order to evaluate the enhanced amount of MPI with pump intensity noise, we can assume that the MPI component experiences the different Raman gain when it propagates in different directions. That is to say, the co- and counter-pumping gains of fibre Raman amplifier are slightly changed by the gain fluctuations due to pump-intensity noise [34]. Then, the modified equation for the MPI with pump-intensity noise is given by

$$MPI(L_{eff}) = \left(\frac{S}{\frac{\ln(G_{R\_co}G_{R\_ct})}{\alpha_s L_{eff}} - 2}\right)^2 \left[(G_{R\_co}G_{R\_ct})e^{-2\alpha_s L_{eff}} - 1 - (\ln(G_{R\_co}G_{R\_ct}) - 2\alpha_s L_{eff})\right]$$

where L_{eff} is the effective length of fibre, α_s is the attenuation at the signal wavelength, S is the Rayleigh backscatter capture coefficient, G_{R_co} is the co-pumping Raman gain, and G_{R_ct} is the counter-pumping Raman gain. If MPI is calculated as a function of fibre Raman gain, taking into account the fact that intensity noise levels of commercially available Raman pump laser modules are generally lower than -90dB/Hz, the effect of pump intensity noise on the enhancement of MPI would be negligible. Pump-to-signal crosstalk would be generated by the transfer of pump-intensity noise to signal-intensity noise. It has been reported that pump-intensity noise levels as high as -60dB/Hz are suitable for counter-pumped Raman amplifiers with negligible system penalties. Additionally a high reflection (larger than -20 dB) could enhance the effect of pump-to-signal crosstalk for counter-pumped Raman amplifiers [36], [37].

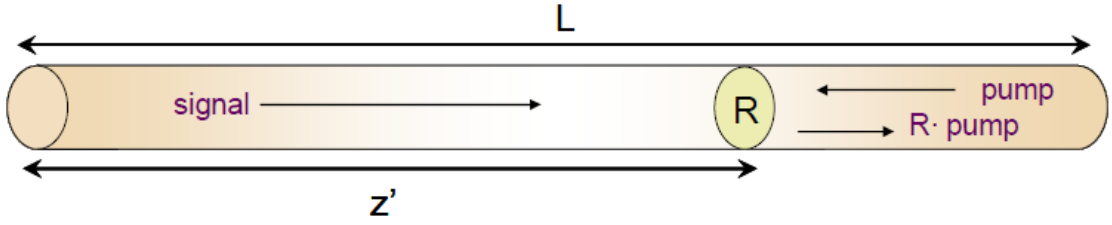

Figure 2-5: Effect of discrete reflectance on pump-to-signal crosstalk for a counter-pumped Raman amplifier. L is the length of fibre, z´ is the reflection point, and R is the discrete reflectance

Assuming that a discrete reflectance of R is located at point z´ in a counter-pumped Raman amplifier, as shown in Figure 2-5, the signal could be reflected by the discrete reflectance at

z´ in both directions; the original signal reflected back to the start of the fibre span and the Rayleigh-backscattered signal reflected to the end of the fibre span. These reflected signals would increase the amount of MPI. The degradation in system's performance could be estimated by using the quality factor (Q) penalties of counter-pumped Raman amplifier as a function of discrete reflectance, reflection point and Raman gain, respectively. In this calculation, transmission through a 100-km long non-zero dispersion shifted fibre was assumed (D = 2 ps/nm/km, αp = 0.25 dB/km) and amplified by using a Raman pump module which had a pump-intensity noise of -90 dB/Hz. Q-penalties would be negligible as long as the value of reflectance was less than -20 dB and the reflection point was located outside the effective length of fibre. It is clear that as reflection point approaches closer to the end of fibre span, a larger amount of residual pump power would be reflected and co-propagated with signal, which in turn causes a larger pump-to-signal crosstalk-induced Q penalty. From the results, we confirmed that the pump-to-signal crosstalk could be enhanced significantly, only when a high reflection (larger than -20 dB) occurred within the effective length of transmission fibre. Therefore, the enhancement of pump-to-signal crosstalk wouldn't be negligible if care hasn't been taken to eliminate all discrete reflections within the effective length of transmission fibre.

2.2.4. Chromatic Dispersion

In an optical fibre, Chromatic Dispersion (CD) is the frequency dependence of the propagation constant β for a given guided mode. This is due to material dispersion, i.e. the frequency-dependence of the refractive index for bulk fibre materials, and to modal dispersion which is the intrinsic frequency-dependence of a guided mode in absence of material dispersion, related to the presence of frequency in the dispersion equation.

When a light pulse propagates into a fibre, chromatic dispersion delays spectral components more than others, thus broadening the pulse both spatially and temporally. This is why CD is typically characterized by the group velocity dispersion *D* expressed as:

$$D \triangleq -\frac{2\pi c}{\lambda^2}\frac{\partial^2 \beta}{\partial \omega^2}(\omega)$$

where *c* is the speed of light in vacuum, λ the wavelength and ω the frequency. By convention, *D*, as a fibre characteristic, is given in ps/(nm.km). This means that for each kilometre of propagation, a 1nm-wide pulse is temporally broadened by *D* picoseconds. Because of temporal broadening, consecutive transmitted symbols tend to merge in the

temporal domain, creating Inter-Symbol Interference (ISI). The main consequence of CD is thus an increased difficulty to distinguish amplitude levels of I/Q signals at reception.

Since shorter symbols are spectrally larger, this effect is all the more important that the baudrate is high. Chromatic dispersion also plays an indirect role in optical transmissions through the way it affects non-linear propagation effects. A major advantage of coherent transmissions for mitigating CD is the phase-sensitivity of the detection, allowing the characterization and correction of CD by relatively simple digital signal processing (DSP) algorithms. With such technique, temporal delays of up to 20,000 ps due to CD - corresponding to thousands of kilometres of propagation - can be easily corrected. One efficient method to compensate for CD is to apply a Finite Impulse Response (FIR) filter to the digitized signals. The filter coefficients are calculated so that filter frequency response precisely compensate the frequency-dependent propagation constant. In simple terms, the filter reverses the effect of CD accumulated during propagation.

2.2.5. Polarization Effects (PMD and PDL)

Single-mode optical fibres actually have two propagation modes, corresponding to orthogonal polarization states. Using these two polarization states doubles the amount of data that can be transmitted through a single-fibre, provided that the signals carried by each polarization can be separately detected at reception. Polarization effects such as Polarization-Mode Dispersion (PMD), Polarization-dependent-Loss (PDL) and Polarization Rotation (PR), by individually modifying and coupling signals carried by orthogonal polarizations with complex coefficients, make polarization demultiplexing paramount for recovering independent input signals at reception. The effects of PMD, PDL and PR are best described introducing Jones formalism. Input and output polarization states S_{IN} and S_{OUT} are modelled by two-dimensional vectors in an orthonormal basis. The polarization-state transformation occurring during transmission from transmitter to receiver is described by a 2x2 complex matrix *M*:

$$S_{OUT} = MS_{IN}$$

$$\begin{pmatrix} S_{X,OUT} \\ S_{Y,OUT} \end{pmatrix} = \begin{pmatrix} A & B \\ C & D \end{pmatrix} \begin{pmatrix} S_{X,IN} \\ S_{Y,IN} \end{pmatrix}$$

A, *B*, *C*, *D* are complex coefficients. We point out here that, whereas *A* and *D* are only responsible for independent signal modifications, B and C directly appear as coupling coefficients between the initially independent signals $S_{X,IN}$ and $S_{Y,IN}$.

1. Polarization Rotation (PR)

Polarization rotation is the most simple polarization effect to understand. If we neglect all forms of impairments between transmitter and receiver, matrix *M* will be reduced to a rotation matrix R_θ describing the angular misalignment θ between PSPs on both sides. Such matrix is thus written:

$$R_\theta = \begin{pmatrix} \cos\theta & -\sin\theta \\ \sin\theta & \cos\theta \end{pmatrix}$$

Thus, even in an ideal case, received signals $S_{X,OUT}$ and $S_{Y,OUT}$ will both be a linear combination of input signals $S_{X,IN}$ and $S_{Y,IN}$.

2. Polarization-Mode Dispersion (PMD)

The term "polarization-mode dispersion" (PMD) relates to fibre birefringence effects that have a common consequence: a phase-delay between signals carried by the two polarization states of a fibre. Birefringence, either fibre-intrinsic - due to imperfect rotational symmetry of the fibre - or due to environmental factors (mechanical constraints, temperature gradients, etc.), causes polarization modes to propagate at different speeds, hence the resulting phase-delay. As such, PMD causes a non-zero and time-dependent Differential-Group-Delay (DGD), defined as the difference of group delays between waves propagating along the two polarizations modes, and expressed in ps. It is important to point out that consecutive DGD values are not deterministic: they are well described by a Maxwellian probability density function. Therefore, it is the DGD average, also called PMD (ps), which is most commonly used to characterize the effect of birefringence in any optical device of a communication system. In Jones formalism, the action of PMD can be modelled by a matrix M_{PMD}, as:

$$M_{PMD} = \begin{pmatrix} e^{-i\varphi/2} & 0 \\ 0 & e^{+i\varphi/2} \end{pmatrix}$$

where φ is the frequency-dependent phase-delay accumulated between waves propagating along the two Principal States of Polarization (PSP). Intrinsically, PMD does not cause coupling of input signals. However, there is no reason why fibre PSPs would be aligned with transmitter and receiver PSPs. Therefore, in a common orthonormal base, it is preferable to write the PMD matrix M^*_{PMD} as:

$$M^*_{PMD} = R_\alpha \begin{pmatrix} e^{-i\varphi/2} & 0 \\ 0 & e^{+i\varphi/2} \end{pmatrix} R_\beta$$

where R_α and R_β are rotation matrices. These rotation matrices are responsible for coupling the input signals together in addition to the phase-delay effect due to PMD.

3. Polarization-Dependent Loss (PDL)

Unlike PMD, polarization-dependent loss (PDL) does not affect the relative phase between waves propagating along orthogonal polarization states. PDL modifies their relative amplitudes. In a fibre, PDL can be due to a slight variation of optical attenuation depending on the polarization state. However, in optical communication systems, most PDL come from other elements: filters, switches, amplifiers, etc... As a result, an important imbalance in quality (measured by signal-to noise ratio) between signals $S_{X,OUT}$ and $S_{Y,OUT}$ can be observed at reception. PDL can be modelled for any device, fibre and others, as a diagonal matrix M_{PDL} in the orthonormal matrix formed by the PSPs of the device, as:

$$M_{PDL} = \rho \begin{pmatrix} \sqrt{1-k} & 0 \\ 0 & \sqrt{1+k} \end{pmatrix}$$

where ρ^2 characterizes the lump energy loss of the considered device, and the k describes the unequal distribution of loss according to input polarization state. Both ρ and k are real positive coefficients with values ranging from 0 to 1. Similarly to the case of PMD, we can also write M_{PDL} as a non-diagonal matrix M^*_{PDL} in a non-specific orthonormal base to take into account misalignments between Rx, Tx and device PSPs.

Polarization-multiplexing would probably be impossible without efficient schemes to mitigate the polarization effects described above. Indeed, in the worst cases, received signals would be a complex and equitable mix of direct and delayed versions of both input signals. Since PMD, PDL and PR effects from multiple optical elements are typically combined in between transmitter and receiver, it would be very complicated to correct them separately. For this reason, most employed technique is based on blind signal equalization, using a Constant Modulus Algorithm to invert the matrix M and recover input signals independently from each other. Rapidly and randomly varying birefringence leads to PMD (polarization mode dispersion), that can be described by Coupled Nonlinear Schrödinger Equation, or the Manakov equation which can be derived from the coupled nonlinear Schrodinger equation and is fully equivalent to it [38]. Its use is appropriate when modelling optical fibres whose birefringence orientation changes rapidly by comparison with the typical length scales for chromatic dispersion, polarization mode dispersion, and nonlinearity. The Manakov equation consists of a set of terms that correspond physically to linear PMD, chromatic dispersion, the Kerr nonlinearity, and nonlinear PMD.

PMD is an important parameter to be monitored to avoid network outage. However, in coherent transmission the use of adaptive digital filter for PMD compensation has made PMD monitoring much less critical. Linear PMD can be (at least partially) compensated at the DSP by the CMA algorithm. The measured DGD could fluctuate on an hourly or daily timescale, but there should be little or no parameter drifts due to fibre ageing.

In optical systems, PDL comes from the small anisotropy induced by non-ideal physical elements such as fibre slicing and optical components [38]. These elements are spread along the optical link and the contribution of each element can change over time due to aging, faults, maintenance activities etc. When many PDL elements are linked together by optical fibres, the end-to-end transmission properties in terms of total PDL and insertion loss become statistical quantities. In practice, spontaneous emission noise that is generated by optical amplifiers along the link becomes partially polarized and fluctuates due to PDL concatenation. The fluctuations of noise, signal power, and path average power all affect the quality of the transmitted signal. Consequently, PDL may be modelled via a random process; its impact is then usually studied using the outage probability [39]. In PDL-impaired transmission systems, coding schemes using both Polarization-Time (PT) codes and Low-Density Parity Check (LDPC) codes can be usefully employed. PT codes are space-time codes applied to polarization-multiplexed systems, and have been widely advocated for PDL mitigation: spreading the information symbols over time and both polarizations partly counteracts the uneven energy repartition amongst the polarizations. An LDPC code can complement them to further improve BER performance. Delesques et al. [40] have compared the outage probability to the BER offered by simulated systems using QPSK modulation and several coding schemes: LDPC and/or PT Codes, or no coding. These simulations have shown that PT codes are more robust to PDL than LDPC, and that the concatenation of a PT code with an LDPC is even better. They found that for a mean PDL of 3 dB, a simulated system based on PT and LDPC codes (with soft decoding) performs with an SNR gap of only 1.5 dB to the fundamental limit. While more powerful coding schemes could undoubtedly edge closer to the limit, the modest 1.5 dB gain that can be hoped for must be balanced against the computational complexity, which is already the major drawback of LDPC soft decoding, especially at the very high bit rates. Polarization Dependent Loss and Gain effects in coherent systems have become available only recently [39],[41]. In particular, Zamani et al [39] show that PDL/PDG induced penalty can be relatively small in dual polarization coherent systems provided that Polarization-Time (PT) codes are used.

Based on these results, and assuming that PT codes are implemented in coherent systems, one could adopt the following approach:

- adding a 0.2 dB OSNR margin for DP-16QAM and DP-64QAM modulation formats whose reach is shorter than 7 amplification sections and therefore may be affected just by limited PDL/PDG (<2 dB);
- adding a 0.5 dB OSNR margin for DP-BPSK and DP-QPSK modulation formats whose reach is up to 33 amplification sections and therefore may be affected by medium PDL/PDG (<4 dB).

Cumulative filtering effects in flexgrid ROADM require further studies. For the time being a tentative estimation of the related penalty is:

- 0.5 dB OSNR penalty for DP-16QAM and DP-64QAM modulation formats (due to their shorter reach they are expected to pass through a limited number of ROADMs);
- 1 dB OSNR penalty for DP-BPSK and DP-QPSK modulation formats (due to their long reach they are expected to pass through a significant number of ROADMs).

Table 2-2: Various typical margins according to the modulation format of the transmission

Modulation format	Rx OSNR sensitivity w/o margin [dB]	Power equalization margin [dB]	PDL/PDG margin [dB]	Cumulative filtering margin [dB]	Rx OSNR sensitivity with margin [dB]
DP-BPSK	9.41	1	0.5	1	11.91
DP-QPSK	12.42	1	0.5	1	14.92
DP-16QAM	19.48	1	0.2	0.5	21.18
DP-64QAM	25.82	1	0.2	0.5	27.52

2.2.6. Spectral Distortion (e.g. due to cascaded filtering)

The effect of cumulative filtering on optical signals due to the crossing of many Bandwidth Variable Wavelength Selective Switches (BV-WSS) in an elastic optical network (EON) imposes constraints on the bandwidth that can be allocated for each channel. This may have a significant impact on the expected spectral efficiency of an EON based on flexgrid. If narrow filters are used, penalties are much higher than those mentioned above [42].

The impairment, however, appears to be less severe on super-channels, in comparison to single carrier channels.

Some degree of mitigation can be achieved at the DSP, or better with a digital pre-equalization at the transmitter, or with specially designed filters at each ROADM.

In ROADM systems with power levelling functions, automatic power equalization is performed to counteract OSNR unbalancing between OCh. Still, a fixed OSNR penalty due to

power measurement uncertainty remains and can be estimated as 1dB with today's technologies.

2.2.7. In-band/Out-of-band Crosstalk

Crosstalk or linear Crosstalk is an unwanted effect that appears in WDM optical systems, and more specifically in Arrayed Waveguide Gratings (AWGs), Wavelength Selective Switches (WSS), optical switches and filters and MUX/DEMUX devices. It refers to the interference caused in a propagating signal from the neighbouring channels due to the dense WDM channel spacing and is classified as in-band and out-of-band crosstalk. It is considered linear as it corresponds to the power transferred due to an imperfection in the WDM components rather than the nonlinearity of optical channels.

Out-of-band Crosstalk

Out-of-band crosstalk refers to the inflicted interference due to neighbouring channels at different wavelengths. It is a result of the imperfect filtering of signals outside of the spectrum of the investigated signal and it appears both in all the aforementioned optical subsystems since all of them employ filtering. As shown in Figure 2-6, due to the narrow spacing of several WDM channels, imperfect filtering fails to cut off all channels apart from the channel selected. A part of the neighbouring channel's spectrum lies in the passband of the filter and, as a result, the residual spectrum interferes with the selected channel.

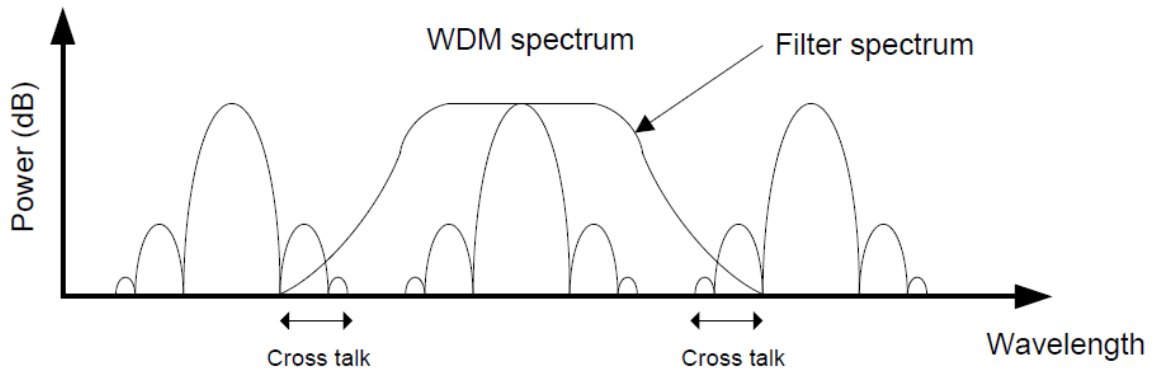

Figure 2-6: Illustrating out-of-band crosstalk [43]

In-band crosstalk noise arises from imperfections in optical cross-connects. An attenuated and delayed version of the signal, or a small portion of light from other channels at the same wavelength (in a network with wavelength reuse), is routed along the same path as the signal. Since in-band crosstalk noise is at the same wavelength as the signal, it cannot be removed using additional filtering and can degrade the BER at the receiver.

In a similar manner, filtering and channel selection in an optical switch, AWG, or WSS would result in out-of-band crosstalk between the outputs. In Figure 2-7, a 1x5 WSS is fed with signals at several wavelengths. In this example, out-of-band crosstalk would exist between signals at different wavelengths, but exiting at the same output.

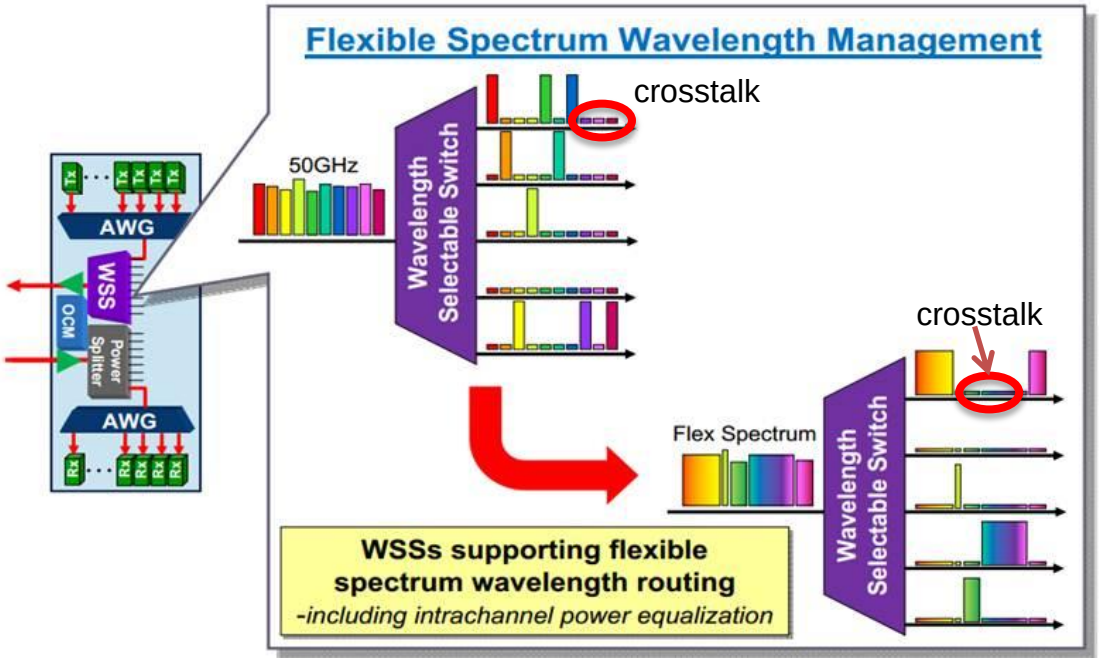

Figure 2-7: A WSS with unwanted signal power (crosstalk) at all ports, for fixed- (top) and flexible spectrum configurations (main figure originally published in [44]).

In-band Crosstalk

In-band crosstalk noise arises from imperfections in optical cross-connects such as the AWG routers described above. An attenuated and delayed version of the signal, or a small portion of light from other channels at the same wavelength, is routed along the same path as the signal. The effect of interfering connections at the same wavelength is more severe because of its coherent nature that causes the interference to occur within the receiver bandwidth.

Since in-band crosstalk noise is at the same wavelength as the signal, it cannot be removed using additional filtering and can degrade the BER at the receiver. In contrast, out-of-band crosstalk can be mitigated by suitable filtering at the receiver, as this kind of interference has an incoherent nature and depends only on the power of the neighbouring wavelength [45].

2.3. Nonlinear Effects

All nonlinear effects are described by the Nonlinear Schrödinger Equation (or the Manakov Equation taking into account polarization) through the parameter γ, i.e. the ratio between the silica Kerr nonlinear refractive index n_2 and the fibre effective area A_{eff}. Backward

propagation method is the method that a DSP could use to mitigate intra-band nonlinear effects. An effective γ parameter (different kind of fibres could make up the link) could be a by-product of this algorithm. Also γ is little or no dependent on fibre ageing. In a long haul transmission link with chromatic dispersion (CD) and fibre nonlinearity, it is difficult to distinguish between amplifier noise and fibre nonlinearity induced distortions from received signal distributions after applying various transmission impairment compensation techniques, thus resulting in grossly inaccurate OSNR estimates. Based on the received signal distributions after carrier phase estimation (CPE), Zhenhua Dong et al. [46] propose to characterize the nonlinearity-induced amplitude noise correlation across neighbouring symbols and incorporate such information into error vector magnitude (EVM) calculation to realize fibre nonlinearity-insensitive OSNR monitoring.

A different approach is to treat nonlinear impairments as an effective noise: the analytical model described in [47], [48] has been shown to compare very well with numerical simulations and experimental data. The system performance is quickly predicted through a closed-form analytical formula. Although the model has been tested extensively against PM-QPSK transmission simulations, its validity is not limited to this format, and can be used with PM-QAM or other coherent modulation formats as well.

When nonlinear effects can be treated as a perturbation, the statistical distribution of each of the constellation points (after the DSP has compensated for linear effects) appears to be Gaussian, even without added ASE noise. Based on this, nonlinear impairments are accounted for by means of an effective power, P_{NLI}, to be added to ASE power, P_{ASE}. The BER depends on an effective OSNR, modified to account for nonlinear propagation effects:

$$OSNR_{eff} = \frac{P_{TX}}{(P_{ASE} + P_{NL})}$$

P_{NL} was found to have a cubic dependence on power, $P_{NL} = N_{span}\eta\gamma^2 P_{TX}{}^3$ where γ is the fibre nonlinear coefficient, N_{span} is the number of spans, η is a parameter that depends on system parameters, such as baud-rate, channel spacing, span length and fibre chromatic dispersion. It can be fitted from simulations, or computed numerically through a double integral [47].

It is to be noted that the model presumes low to moderate nonlinearity, and works better for long links (where chromatic dispersion has effectively 'randomized' the nonlinear interactions). It is remarkable that once η has been determined, the system behaviour can be predicted for a wide range of situations.

Considering, as usual, a link where in-line amplifiers completely recover fibre loss, the ASE power is given by $P_{ASE} = N_{span} A_{span} FhfB$, where A_{span} is the span loss, *F* is the noise figure,

h is the Planck constant, *f* the operation frequency, *B* the equivalent noise bandwidth over which OSNR is evaluated. The above formula becomes:

$$OSNR_{eff} = \frac{P_{TX}}{N_{span}(A_{span}FhfB + \eta\gamma^2 P_{TX}{}^3)}$$

After $OSNR_{eff}$ is computed, it is possible to estimate the system performance in terms of the maximum span loss or maximum number of spans (and then the maximum distance), by imposing that it is at least equal to the OSNR that is required in order to achieve the target BER. Using this expression for $OSNR_{eff}$, the maximum number of spans for a fixed transmission power can be derived once a target OSNR, corresponding to a target BER, is established (experimentally or via simulations).

An optimum value for the transmission power, that maximizes the number of amplification spans, can be derived in this analytical scheme [48]:

$$P_{TX,opt}^{Nspan} = \left[\frac{A_{span}FhfB}{2\eta\gamma^2}\right]^{1/3}$$

An interesting result deriving from this kind of analysis is that at the optimum transmission power the amount of ASE noise is always twice the amount of non-linear noise: P_{ASE} = 2 P_{NL}. Another interesting feature is that the maximum reachable distance in nonlinear propagation is always equal to 2/3 of the distance the system could reach in linear regime, at the optimum launch power:

$$N_{span}^{\max} = \frac{1}{OSNR_{target}}\left(\frac{2}{3}\right)\left(\frac{P_{TX,opt}^{Nspan}}{A_{span}FhfB}\right)$$

Once the required receiver sensitivity $OSNR_{target}$ is set, the feasibility of a given optical link can easily be established. Calculation of η is cumbersome, but a practical approximate expression can be used:

$$\eta \approx \left(\frac{2}{3}\right)^3 \frac{L_{eff}^2}{L_{eff,a}\pi\beta_2 B_{ch}^3} a\sinh\left(\frac{23}{5}\beta_2 L_{eff,a} B_{ch}^2 \left[N_{ch}^2\right]^{\frac{B_{ch}}{\Delta\nu}}\right)$$

With channels that have a rectangular spectrum, and spacing equal to the spectral width (*Nyquist* DWDM), aggregate DWDM spectrum id flat and η becomes:

$$\eta \approx \left(\frac{2}{3}\right)^3 \frac{L_{eff}^2}{L_{eff,a}\pi\beta_2\Delta\nu^3}\, a\sinh\left(\frac{23}{5}\beta_2 L_{eff,a} B_{ch}^2 N_{ch}^2\right)$$

If noise contributions coming from different amplification spans are not independent of each other, the formula can be modified to:

$$OSNR_{eq} = \frac{P_{Tx}}{N_s a_s NFh\nu B_n + N_s^{1+\varepsilon}\gamma^2\eta_{NL}P_{Tx}^3}$$

The parameter ε describes how nonlinear noise cumulates along the link. A good approximate expression for it is:

$$\varepsilon \cong \frac{3}{10}\log\left(1+\frac{6}{L_s}\frac{L_{eff,a}}{asenh\left(\frac{23}{5}\beta_2 L_{eff,a} 0.9^2 B_{ch}^2 \left[N_{ch}^2\right]^{\frac{B_{ch}}{\Delta\nu}}\right)}\right)$$

And the power that maximizes $OSNR_{eff}$ becomes:

$$P_{Tx,opt} = \sqrt[3]{\frac{N_s a_s NFh\nu B_n}{N_s^{1+\varepsilon}2\gamma^2\eta_{NL}}} = N_s^{-\varepsilon/3}\sqrt[3]{\frac{a_s NFh\nu B_n}{2\gamma^2\eta_{NL}}}$$

The optimal OSNR becomes:

$$OSNR_{eq,opt} = \frac{P_{Tx,opt}}{N_s a_s NFh\nu B_n + \frac{1}{2}N_s a_s NFh\nu B_n} = \frac{N_s^{-\varepsilon/3}\sqrt{\frac{a_s NFh\nu B_n}{2\gamma^2\eta_{NL}}}}{\frac{3}{2}N_s a_s NFh\nu B_n}$$

Although some works about OPM in the literature focuses in disentangling the nonlinear contribution to the noise (and OSNR), the approach described above is enough to evaluate system performances from an effective OSNR.

Table 2-3 shows typical values of ε in DWDM systems (80 channels, 50 GHz spaced, span length 90 km) for three different kinds of fibre.

Table 2-3: Typical values of fibre coefficients according to fibre model

Fibre type	**SMF**	**PSCF**	**NZD**
Beta2 [s^2/km]	2,17E-23	2,55E-23	4,84E-24
Attenuation coefficient [dB/km]	0,22	0,17	0,22
Effective Length [km]	19,74066	25,54673	19,74066
Epsilon	0,05149	0,061772	0,064041

Corrections to optimal power and $OSNR_{eq}$ are around 0.2 to 0.3 dB for the values in Table 2-3, and a number of amplification spans ranging from 10 to 30, typical of terrestrial systems. Maximum number of spans can be evaluated as:

$$N_{s,\max} = \left(\frac{\sqrt[3]{\frac{a_s NFh\nu B_n}{2\gamma^2 \eta_{NL}}}}{OSNR_{eq,req} \frac{3}{2} a_s NFh\nu B_n} \right)^{\frac{1}{1+\varepsilon/3}}$$

Further investigations are needed to potentially isolate ASE noise, SPM and XPM, although this could be unnecessary for many practical purposes.

2.3.1. Self-Phase Modulation (SPM)

Self-Phase Modulation is a phenomenon induced by the Kerr non-linear effect. This effect refers to the intensity dependent change of the refractive index which can be expressed by:

$$n = n_0 + n_2 \frac{P(t)}{A_{eff}} \quad (3)$$

Where n_0 is the linear refractive index, $P(t)$ is the optical power in Watt, A_{eff} is the effective area in m^2 and n_2 the non-linear refractive index in m^2/W. Although the value of n_2 is typically small in an optical fibre is still non-negligible due to small A_{eff}. According to (3), the phase of an optical signal travelling in a medium with power-dependent refractive index can be represented as:

$$\varphi(z,t) = \frac{2\pi z}{\lambda} n = \frac{2\pi n_0 z}{\lambda} + \frac{2\pi n_2 z_{eff}}{\lambda} \frac{P(t)}{A_{eff}} \quad (4)$$

Where z_{eff} is the effective length of fibre that corresponds to the lossless fibre length over which nonlinearities take effect:

$$z_{eff} = \frac{1 - e^{-az}}{a} \quad (5)$$

In (4), the power-dependent refractive index causes a nonlinear phase shift proportional to the signal power and the effective length. This nonlinear phase shift modulates the phase of signal itself and therefore is called self-phase modulation (SPM). Consequently, SPM induced phase shift is defined as:

$$\varphi_{SPM}(z,t) = \frac{2\pi n_2}{\lambda} P(t) z_{eff} = \gamma P(t) z_{eff} \quad (6)$$

This time-dependent phase variation leads to a frequency shift computed by the derivative over time of (5), implying a spectral broadening effect.

Moreover, in the presence of chromatic dispersion the frequency shifted components will either enhance (when $D < 0$, normal dispersion regime) or reduce (when $D > 0$, anomalous dispersion regime) pulse broadening. Note that the SPM effect is more significant at the beginning of a span where the signal power is higher.

Various schemes for SPM mitigation (and generally for Kerr non-linearities compensation) have been proposed on the literature such as Volterra series based equalizer [49], radio-frequency (RF)-pilot tone technique [50], [51], phase-conjugated twin waves [52] and the digital back-propagation algorithm (DBP) [53]. Extended research has been conducted for the latter technique of DBP which is capable for joint compensation of linear and nonlinear effects. Although, the main limitation of this method is its hardware requirements which prohibits an implementation for real time coherent systems.

2.3.2. Four Wave Mixing (FWM)

Four wave mixing is a phenomenon in which three waves at different frequencies (ω_1, ω_2, ω_3) can interact via the third order nonlinear susceptibility to generate a fourth wave at frequency $\omega_4 = \omega_1 + \omega_2 - \omega_3$ (this condition expresses the conservation of energy of the involved photons). A special case of four wave mixing occurs when two photons at the pump frequency and one photon at the idler frequency are converted into a photon at the signal frequency $\omega_\sigma = \omega_\pi + \omega_\pi - \omega_i$. In order to achieve an effective power transfer, momentum must also be conserved: this is called phase matching condition and reads:

$$\delta k = \frac{n_1\omega_1}{c} + \frac{n_2\omega_2}{c} - \frac{n_3\omega_3}{c} - \frac{n_4\omega_4}{c} = 0 \quad (7)$$

where *c* is the speed of light and n_1, n_2, n_3, n_4 are the refractive indexes at the corresponding frequencies. Since this condition involves the refractive index at different wavelengths, it is more easily satisfied near the zero dispersion wavelength of the fibre.

Recently, to address perturbative models for the impact of nonlinear propagation in uncompensated links, the signal has been split up into spectral components and then a four-wave-mixing-like approach has been employed to assess the generation of nonlinear interference due to the beating of the signal spectral components [54]. A significant set of formats encompassing PM-BPSK, PM-QPSK, PM-8QAM, and PM-16QAM at 32 GBaud were numerically simulated in order to validate the model prediction of maximum system reach and optimum launch power versus simulation results. The model delivers accurate predictions, potentially making it an effective general-purpose system design tool for coherent uncompensated transmission systems.

2.3.3. Cross-Phase Modulation (XPM)

Cross-Phase Modulation can occur when several optical channels share the same fibre, for instance in high-capacity DWDM networks. Because of Kerr effect, for one given channel, the refractive index of the fibre varies as a function of its own power (which causes SPM), but also varies a function of the powers from all other channels propagating in the same fibre. This causes XPM. In a first XPM model, each additional channel *p* of amplitude $A_p(z,T)$ introduces a local variation of fibre refractive index at *z* and instant *T* as:

$$\delta n(z,T) = 2n_2 \frac{\left|A_p(z,T)\right|^2}{A_{eff}}$$

where A_{eff} is the fibre effective section and n_2 is the fibre Kerr coefficient.

In the usual case where all channels have equal powers, this model predicts the XPM to be twice stronger than SPM. However, this is a scalar model, not taking into account the vector nature of the electric field. A more realistic ratio between XPM and SPM would be 1.5.

All temporal variations of additional channels induce index variations - thus phase variations - in the studied channel. As consequence, its spectrum can be broadened, and distorted as a combined effect with chromatic dispersion. However, contrary to SPM, XPM is not

deterministic since index variations depend on the information carried by other channels. Considering that other channels propagate at different speeds than the studied channel, the phase match condition, necessary for the nonlinear effect to occur, is seldom realized for additional channels beyond those directly adjacent to the studied channels.

2.3.4. Cross-Polarization Modulation (XPolM)

Cross-polarization modulation (XPolM) is an inter-channel effect resulting in fast polarization-modulation of signals and therefore to a depolarization of the transmitted signal, resulting in fading and channel cross-talk for dual-polarization (DP) signals. Looking at a particular channel, XPolM-induced depolarization depends on the variance of the Stokes vector of the aggregate co-propagating channels. Expressed in Stokes space, the variation of the state of polarization (SOP) of the investigated channel *a* due to channel *b*, is given by [46]:

$$\frac{\partial \overrightarrow{s_a}}{\partial \vec{z}} = \frac{8}{9}\,\gamma \overrightarrow{s_a} \times \overrightarrow{s_b} \tag{8}$$

where $\boldsymbol{s_a}$ and $\boldsymbol{s_b}$ are the Stokes vectors of channel *a* and channel *b*, respectively. The fact that the state of polarization of the investigated channel, as well as the neighbouring channels evolve randomly over the transmission due to CD and PMD, makes the XPolM effect pattern-depended and stochastic [55]. Nonlinear polarization scattering causes the SOP to change at the speed of the symbol rate, which is hard to follow with DSP in coherent receivers, and may induce severe crosstalk between two polarization tributaries. The resulting penalty has been predicted to be particularly important for dual-polarization (DP) signals deployed over legacy DM systems. In coherent optical communication systems with DCF, when modulation formats of constant amplitude such as QPSK are used, the dominant nonlinear effect is XPolM, whereas when the channels carry non-constant amplitude modulation formats such as hybrid QPSK and OOK or 16-QAM, XPM is the dominant nonlinear effect.

In [56] a transmission experiment investigates the XPolM penalty of a 42.8-Gb/s and 112-Gb/s NRZ-PDM-QPSK channel surrounded by six 21.4-Gb/s and 56-Gb/s NRZ single-polarization (SP) QPSK channels, which have the same symbol rate as the PDM-QPSK channel. The results indicate that XPolM is the dominant nonlinear effect in the homogeneous NRZ-PDM-QPSK system with DCF, and it is XPolM that makes homogeneous PDM-QPSK systems with DCF perform worse than those without DCF. The reason why the PDM-QPSK channels cause less inter-channel penalty than SP-QPSK channels in the systems without DCF is because the impact of the inter-channel XPM is much larger than XPolM in these systems, and the peak powers of PDM signals are smaller than those of SP signals for a

given average power, due to different data in the two polarizations of the PDM signals. A similar result was also shown in [57] where different nonlinearities are compared in DM links.

2.3.5. Raman Amplification

Raman amplification exploits stimulated Raman scattering, involving phonons, i.e. acoustic vibrations of the medium; the frequency difference between Raman pump and signal, 13.2THz at the gain peak in silica, is independent from the signal wavelength. Gain spectrum is tens of nanometres wide, flat enough to allow the realization of wide band amplifiers. Differently from EDFA, amplification requires many fibre kilometres; besides, one can build amplifiers in any spectral region of interest provided an appropriate pump wavelength is selected. Using more than one pump wavelength can further improve gain spectrum flatness. Co-propagating and counter-propagating (or both) pump-signal configurations can be used, counter-propagating configuration being more effective in reducing pump power fluctuations.

In case of counter-propagating pumping, simple formulas can be derived for on/off gain (i.e. net gain accounting also for span loss):

$$G_{tot} = e^{\int_0^L C_{R;\nu_P,\nu_S} P^-_{P;\nu_P}(z)dz} \cdot e^{-\alpha_S L} = G_{on/off} A$$

$$G_{on/off} = Exp\left(\int_0^L C_{R;\nu_P,\nu_S} P^-_{P;\nu_P}(z)dz\right) \underset{no\ sat.}{\cong} Exp\left(C_{R;\nu_P,\nu_S} P^-_{P;\nu_P}(L)\frac{1-e^{-\alpha_P L}}{\alpha_P}\right)$$

And for noise:

$$P_{Noise}(L) = 2\left(h\nu_S \Delta\nu\, N_{T;\nu_P,\nu_S}\right) C_{R;\nu_P,\nu_S} G_{tot} \cdot \int_0^L \frac{P^-_{P;\nu_P}(z)}{G_{tot}(z)} dz$$

Where $\Delta\nu$ is the signal bandwidth, $C_{R;Vp,Vs}$ is the Raman gain coefficient, depending from the frequency difference between pump and signal and the kind of fibre.

The term $(1-e^{-\alpha_p L})/\alpha_p$ defines an effective length (L_{eff}, P) rapidly reaching an asymptotic value for fibre lengths greater than 50 km.

$$N_{T;\nu_P,\nu_S} = \left[1 + \frac{1}{\left(\exp\left[\frac{h(\nu_P-\nu_S)}{kT}\right]-1\right)}\right]$$

Is the phonons thermal noise contribution to spontaneous emission noise, increasing the noise of about 20% at room temperature. Neglecting pump saturation, and assuming the same value for pump and signal attenuation (e.g. an intermediate value), a simple analytical formula applies:

$$P_{noise}(L) \cong 2h\nu_S \Delta\nu N_T \left(1+\frac{\alpha}{C_R P_P(L)} e^{\alpha L}\right) G_{on/off} - \left(1+\frac{\alpha}{C_R P_P(L)}\right)$$

Figure shows small signal on/off gain behaviour as a function of wavelength, for different kinds of fibre (single counter-propagating pump at 1455 nm, with 700 mW power, 100 km fibre length; signal input power is as low as 1 mW, to avoid pump depletion that would bring to gain saturation.

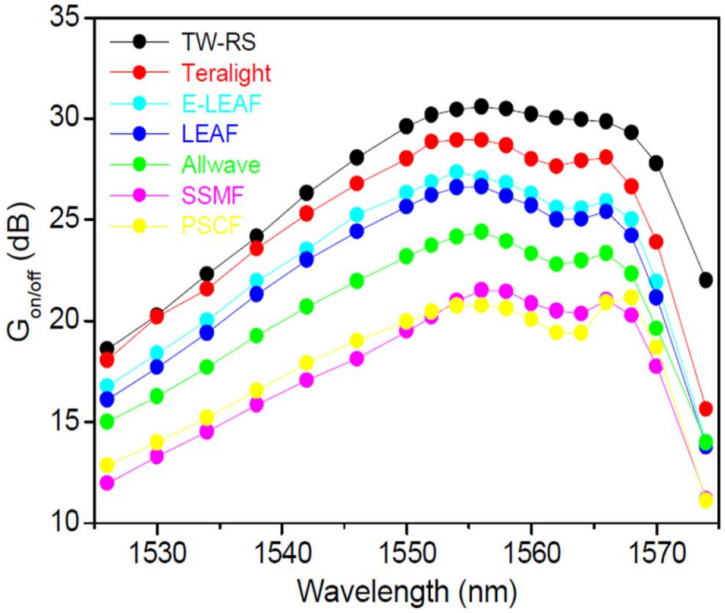

Figure 2-8: On/off gain behaviour vs. wavelength, for different kinds of fibre (single counter-propagating pump at 1455 nm, with 700 mW power, 100 km fibre length

Usually Raman amplification is associated to EDFA in high attenuation spans. Spontaneous emission noise is computed by summing the contribution of the two amplifiers:

$$P_{ASE,i} = P_{R,noise,i} \cdot G_{EDFA,i} + NFh\nu B_N G_{EDFA,i}$$

where $P_{R,noise,i}$ is computed with $\Delta\nu=B_N$, once an appropriate value of the Raman gain has been chosen. $G_{EDFA,i}$ in the first term of this expression refers to amplification of Raman noise by the EDFA section.

3. Why pulse shaping for cost sensitive metro networks should differ from optimal pulse shaping for long-haul networks

The work presented in this section led to publication [58].

As capacity demands continue to grow, there is little doubt that coherent technologies from long-haul networks will largely expand into metro networks. However, they need to be tailored for metro, and to achieve lower-cost operation [60], [61].

In metro networks, the most prominent impairments often stem from the optical filters found in consecutive nodes. Spectral bandwidth reduction and relative laser-filter detuning directly translate into optical signal-to-noise ratio (OSNR) penalties. It is made worst in metro networks due to lesser quality of deployed filters and lasers. To cope with these penalties, containing the signal spectral occupancy as well as in long-haul networks, by digital pulse preshaping in the transmitter with digital to analogue convertors (DAC) is tempting, as DACs come with minimal extra cost in the transponder ASIC which performs signal processing.

Here, we experimentally investigate penalties introduced by the filter cascade, while accounting for relaxed frequency specifications of laser and filters in metro networks, both in terms of bandwidth and central frequency mismatch. We show that Nyquist digital pulse preshaping, as optimized for minimal spectral occupancy as in long-haul networks is often not desirable in metro networks.

3.1. Experimental Setup

We assume that future metro networks will likely carry dynamic traffic, making colorless and directionless ROADM nodes attractive [60]. We therefore emulate route-and-select nodes out of a pair of wavelength selective switches (WSS). They are configured to accommodate channels every 50GHz, as required in highly-capacity future metro networks. Since, before multiplexing, individual channels are filtered once, we only consider a single channel and neglect crosstalk. We insert the WSSs into a recirculating loop as shown in Figure 3-1(a).

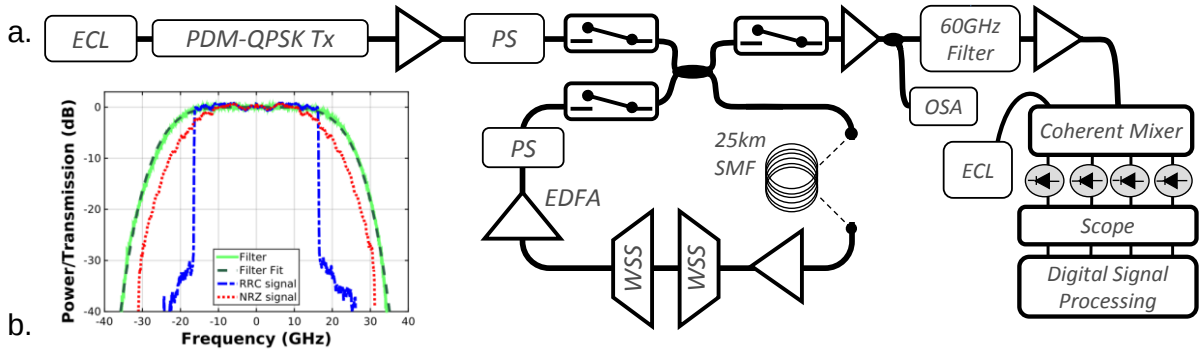

Figure 3-1: (a) Experimental Set-up. (b) Spectrum with Nyquist pulse preshaping (blue dashed line), non-preshaped signal (red dashed line) and filter transfer function of a WSS (green solid line) and its super-Gaussian fit (green dashed line).

At its input, light from an external cavity laser (ECL) is modulated with polarization division multiplexed quadrature phase shift keying (PDM-QPSK) at 32.5GBd, from a 2^{15}-1 pseudo-random binary sequence, including 30% soft-decision FEC and protocol overhead. We consider two pulse types, without preshaping (non-return-to-zero NRZ-like), and with long-haul network-like digital preshaping with root-raised-cosine Nyquist signalling of 0.01 roll-off.

The non-preshaped signal is represented in Figure 3-1(b) with its 65GHz large first lob. In contrast, with a 33GHz rectangular width, most of preshaped signal power fits inside the WSSs' 3dB-bandwidth of 42GHz. WSSs power transfer functions are best approximated by a super-Gaussian[3] of order 2.5, as shown in Figure 3-1(b).

Besides the WSSs, the loop incorporates a polarization scrambler (PS) and 25-km long standard single mode fibre (SMF) spool. The spool generates a small propagation delay between two round trips, large-enough for loop control, while inducing negligible nonlinearity. At loop output, we measure OSNRs in 0.1nm with an optical spectrum analyser (OSA) and receive the signal using a coherent mixer connected to a 40GSample/s oscilloscope with 20GHz electrical bandwidth. We store 100µs-long series of samples and process them offline. After skew adjustments and normalization, we perform polarization demultiplexing using blind equalization based on constant-modulus algorithm (CMA), frequency offset compensation and carrier phase recovery. Finally, we extract the bit error ratio.

3.2. Filtering impact

In this section, we assume the central frequencies of all filters to be perfectly aligned with laser frequency, which we refer as zero-detuning. Figure 3-2(a) reports an OSNR penalty at 2.10^{-2} bit-error ratio, as a function of cascaded filter count, for both signal preshaped with Nyquist signalling and non-preshaped signals. We observe similar penalty profiles for both signal types, matching our previous simulations [42]. The penalty is found to increase supra-linearly with the number of cascaded filters. Even after 60 filters, it remains under 1.4dB. Predictably, data preshaped with Nyquist signalling suffer from smaller penalties than non-preshaped signal, owing to their very small roll-off. Figure 3-2(b) provides some insight on this result. It displays signal bandwidth measurements at 3dB and 10dB from peak, as obtained by calculating the bilateral power spectral density from complex signals, averaging both polarizations. For each filter count, the bandwidth is averaged over five signal acquisitions. Non-preshaped data are found much more sensitive to the number of cascaded filters at 10dB from the peak than at 3dB. It is the opposite for preshaped data. The inherent reason is that filter cascade power attenuation has more impact on signal spectrum for flat regions than for steep-edge regions. At 10dB from peak, preshaped data are much steeper than non-preshaped data; hence the lesser filter effect for preshaped data. At 3dB, preshaped is explaining larger sensitivity of non-preshaped to the filter number. We point out that our experiment only uses a single channel.

3.3. Detuning-based penalties

In a real system, lasers and WSS filters central frequencies are never perfectly aligned with ITU-grid, resulting in significant penalties. For both, frequency misalignments may affect all devices differently because of manufacturing variability. Aging causes additional, time-dependent detuning. In core networks, high-priced lasers and WSSs are typically guaranteed with frequencies within ±1.5GHz and ±2.5GHz of the nominal value, respectively. Next we evaluate the impact of frequency misalignment not only for these costly versions, but also for lesser-quality devices for metro networks.

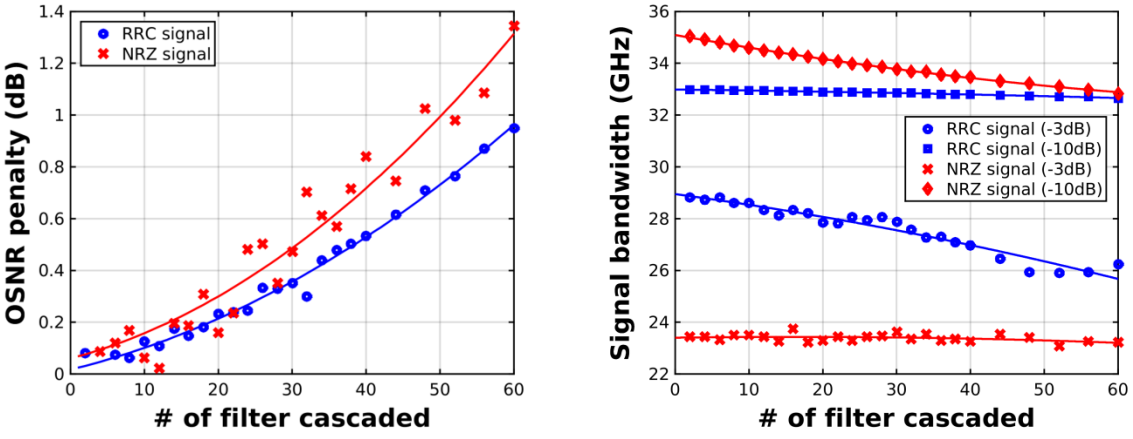

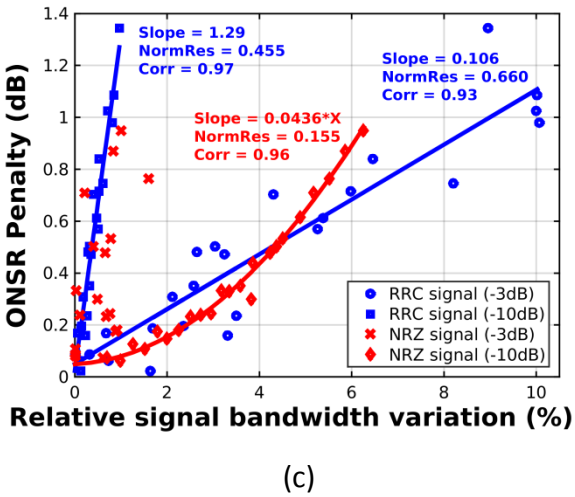

(c)

Figure 3-2: (a) OSNR penalty and (b) 3dB and 10dB signal bandwidth as a function of cascaded filters for Nyquist preshaped and non-preshaped signals. (c) OSNR penalty as a function of detuning between laser and filters for both pulse shapes.

In Figure 3-2(c) we present measured OSNR penalty as a function of laser detuning, up to 6.5GHz, in a scenario where filters are perfectly aligned on ITU-grid. The detuning points are obtained by tuning both emitter and receiver lasers around the central frequency, 193.150GHz here. While more robust to long filter cascades at zero detuning, data preshaped with Nyquist signalling are found less tolerant to detuning than non-preshaped. This suggests optimal pulse shaping should not be solely driven by bandwidth reduction and spectral efficiency as in long-haul networks. It should result in a careful trade-off. Figure 3-3(a) represents the smaller penalty between both signal shapes as a function of cascaded filter count and detuning. Black line shows the separation between regions where non-preshaping outperforms Nyquist preshaping. When detuning is potentially small, Nyquist-

preshaped data performed better, whereas non-preshaped signal is less impaired when detuning is large. Albeit our conclusion was only obtained by forcing laser detuning, we are convinced the conclusion also holds when WSS filters are detuned. Laser detuning can easily be traded for WSS central frequency misalignments. Thus, monitoring of the detuning between the signal and the filter is important to avoid excessive penalty.

3.4. Impairments affecting network resources

To understand how the robustness of signal shaping to filtering and detuning effects acts on the network resources, we dimension a metro network without and with such effects. Given the Gaussian-like signal propagation, 1dB of OSNR penalty after crossing N nodes converts into 1dB of reach penalty [3], having an impact on the achievable optical reach. We consider 1500km [62] as the reference reach for a metro transponder without filter and detuning impairments. Our assumption of route-and-select nodes helps us converting the node count into filter count, while accounting for add/drop (3 filters) and pass-through (2 filters) operations, as explained previously [42].

We considered a meshed metro network [63] with uniform traffic distribution (i.e. all node pairs are chosen with the same probability). To generate a traffic matrix, we start with an empty matrix, and then for a given distribution we draw a random source-destination (s-d) pair. If any path exists between s-d nodes, the demand is added to the matrix; otherwise, blocking occurs and we stop the process deducing the number of demands in the traffic matrix. In a second step, we define the number of required regenerators for a connection in each scenario so as to guarantee the correct connection setup. We remember that in this study we consider a transparent reach that depends on the number of nodes present between two opto-electronic conversions (used for adding/dropping and/or regenerating a signal).

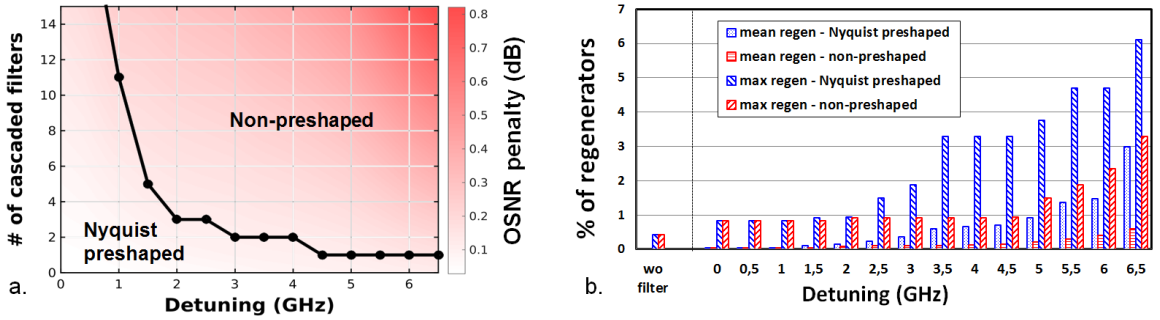

Figure 3-3: (a) Lesser OSNR penalty between preshaping and non-preshaping signal as a function of number of cascaded filters and detuning. Over the black border line, non-preshaped data experience smaller penalties than preshaped data.

Figure 3-3(b) shows the number of required regenerators for preshaped and non-preshaped signals when neither filtering nor detuning is accounted for normalized to the total number of transponders. We observe that all connections can be setup almost transparently (less than 0.5% of regeneration is required) when no filtering effects are considered. Then, we introduced filtering effects (0 detuning), and finally we added detuning effects. We observe that for low detuning values (under 1GHz) the number of additional regenerators is higher if no preshaping is adopted. Conversely, for larger detuning values, non-preshaped signal shows more robustness to detuning degradations. Also, the number of required regenerators has a slower increase than for the preshaped one, which increases exponentially.

Considering a metro environment with lower constraints on frequency accuracy, choosing the right pulse shaping can reduce by up to a factor 2 the number of regenerators needed.

3.5. Conclusions

When tailoring coherent technologies to cost-sensitive, but high-capacity, metro networks, we found that Nyquist signalling with very small roll-off reduces the robustness to likely-significant frequency mismatches between laser and filter devices. Therefore, the best choice for pulse preshaping needs to be tuned to the true optical filters characteristics. This section also shows that filter detuning should be monitored, for instance in order to decrease the D-margins (see Section 1.1).

4. State of the art in monitoring algorithms

4.1. Overview

Network nodes can be generally classified as intermediate nodes and end nodes. At the former, the signal remains in the optical domain and is amplified, filtered and switched. The optical performance monitoring (OPM) that can take place at intermediate nodes is limited to what can be deciphered by the optical amplitude information (e.g. optical power, wavelength and OSNR). The end nodes, which constitute the interfaces between the optical and electrical IP networks, are where conversion to the electrical domain takes place, and the transmitted data are recovered.

In ORCHESTRA, several optimization decisions, such as lightpaths establishment, hard and soft-failure handling, etc. (see use cases in Deliverable D2.1) will be based on information provided by the software-defined optical performance monitoring (soft-OPM) system, enabled by the proliferation of coherent technology. DSP-based digital receivers provide access to amplitude, phase and polarization information, and therefore a host of novel, dynamic soft-OPM functionalities are possible. The challenge is to identify various, often convoluted, impairments based on the received signal. A key parameter to be monitored is the OSNR, as it has a direct and well-known relationship to the BER, and is thus a key indicator of overall performance. As far as CD is concerned, monitoring is less important for current, static networks, since a fixed filter at the receiver is used to compensate for the dispersion, and its coefficients are fixed for a given transmission distance. However, for a dynamic network, CD monitoring is necessary to reduce the time in setting up a lightpath. For PMD, the monitoring system needs to ensure it will not exceed values beyond which the adaptive filter can compensate. In addition, monitoring impairments which can in principle be perfectly compensated by the DSP may also be useful in identifying slowly degrading performance in links due to (e.g.) ageing, and preventing hard failures and outages.

Nonlinear impairments constitute a greater challenge both in terms of compensation, as well as monitoring. While single-channel effects such as SPM can be compensated by techniques such as digital back propagation, implementation complexity of current algorithms is too high to allow real-time application in today's coherent receivers. Inter-channel effects such as XPM are even harder to compensate, since this would depend on obtaining concurrent information from multiple soft-OPM receivers, which is not always a practical situation.

Regardless of the capacity for compensation, monitoring nonlinear impairments is potentially very important for the optimization procedures in flexible optical networks.

4.2. Monitoring of Linear Effects

4.2.1. Signal to Noise Ratio (SNR) and Optical Signal to Noise Ratio (OSNR)

There are many different approaches leveraging DSP algorithms in digital receivers for SNR monitoring. In all cases, what is being measured is the SNR after opto-electronic conversion, and thus includes the noise of the analogue/digital front-end electronics of the coherent receiver (that is, local oscillator and ASE beat noise, thermal noise and shot noise). It is straightforward to calculate SNR from OSNR and vice versa (e.g. [48] and [54]).

The most obvious way of estimating SNR is through the EVM calculation on the equalized and demodulated constellation after the full suite of DSP algorithms have been applied to the received signal. The relationship between EVM and SNR for QAM signals is well known [64]. However, accurate SNR measurement using the EVM depends on the assumption of Gaussian noise and on the accuracy of all preceding DSP stages (e.g. imperfect carrier phase recovery will lead to distortion and affect the estimation).

The monitoring technique proposed in [87] uses equalized training sequences to jointly estimate both PDL and OSNR, based on data-aided 2×2 MIMO FDE. In [66] a method of moments approach is used to estimate the SNR in QPSK signals. This uses the signal magnitude statistics, and can thus be applied prior to frequency offset and carrier phase recovery (but requires polarization demultiplexing/equalization). The scheme of [64] also takes advantage of the signal magnitude characteristics in order to accurately estimate the SNR from an analytically exact expression that relates the mean and variance of the signal magnitude PDFs to the SNR. The method can be applied to any order QAM constellation (not just QPSK) and requires pre-calculation of the analytical SNR expression with a look-up table for real-time monitoring in the Rx DSP. Another method of moments SNR estimator is that of [67]. The closed form expression of the estimator can be implemented real-time for any order QAM.

4.2.2. Chromatic Dispersion

CD estimation and compensation has been widely tackled in research, and is a staple of the coherent digital receiver. A number of data-aided schemes have been proposed, such as the

ones in [68], [69]. Increased bandwidth efficiency can be obtained with non-data aided CD estimation [70],[71], with many techniques relying on scanning over a preset CD range; this is often performed in two iterations, such that a coarse estimate is first obtained with larger scanning steps, followed by a fine-step stage. Techniques not requiring scanning include that of [72] which uses the clock tone power, as well as [73] that uses the autocorrelation of the signal power. The method presented in [74] uses the variance of the optical signal power is used as the monitoring metric for CD. Finally, the adaptive method of [75] relies on a frequency domain equalizer (FDE), a low complexity time domain equalizer (TDE) arranged in the ubiquitous butterfly structure, and an OPM block in a loop configuration. The proposed method aims at exploiting elements already present in the system (TDE, FDE and OPM), and can be applied to networks where the propagation distance can switch dynamically.

4.2.3. Polarization Effects

Methods for estimating PMD are to a certain extent linked to those for CD monitoring, relying on adaptive filter structures (though here are also different approaches, such as the one suggested in [76] that uses the states of polarization as the monitoring signal).

The digital coherent receiver enables equalization, as well as monitoring, of all deterministic linear impairments using the 2×2 butterfly FIR filter structure. After the filters are adapted by a suitable algorithm, a frequency-dependent 2×2 matrix with four elements can be constructed, which correspond to the transfer functions of the adapted filters [77]. This matrix is simply the inverse transfer matrix of the channel and contains combined effects of chromatic dispersion (CD), polarization mode dispersion (PMD) and polarization dependent loss (PDL). Researchers have been addressing the challenge of developing precise algorithms for sorting out the individual impairments. It is possible to monitor CD, first- and second-order PMD and PDL from the monitoring matrix. In the case of second-order PMD, its two components, polarization-dependent chromatic dispersion (PCD) and depolarization (DEP) of the two principle states of polarization (PSPs), the estimation is carried out separately [78],[79].

4.3. Monitoring of Non-Linear Effects

Kerr non-linearities monitoring is the most challenging process envisaged in ORCHESTRA soft-OPM platform. Both SPM and XPM are induced by the interaction of the Kerr effect and the ASE noise from the amplifiers which causes a non-linear phase shift. By exploiting the statistics (mean value and standard deviation) of this phase noise distribution, useful

parameters associated to the optical channel can be determined and used also for the mitigation of these effects [81]. As described on the methodology developed in [82] it is possible to estimate the number of spans and the non-linear coefficient γL_{eff} of an optical link. This estimation process requires the transmission of pilot symbols and can provide the necessary inputs to a non-linear phase noise mitigation scheme such as Digital Back Propagation. As an alternative to the phase distribution statistics, the autocorrelation of the residual received signal phases after the carrier and phase recovery (removal of the linewidth and frequency offset impact) can provide information related to the non-linear behaviour of the optical channel. The investigation of this technique is presented in a related patent by Alcatel Lucent [83].

In the case of a WDM or a multicarrier transmission system the term of XPM is added to the total non-linear phase noise. A reconfigurable optical network has a randomly varying number of adjacent channels (due to the rerouting of lightpaths) thus leading to increased inaccuracy of the above described monitoring process.

5. Experimental investigation of state of the art monitoring algorithms

We report here on the test of an algorithmic method published by Hauske et al [78] using CMA coefficients at the output of the coherent demultiplexer to measure polarization-related parameters, mainly PDL and PMD. We focus on the analysis of a data set from the demodulation of a 32.48GBd PDM-QPSK back-to-back transmission using the same equipment described in section 3. In order to explore the capacity of the algorithmic method to retrieve PMD values, a deterministic PMD source was connected between Tx and Rx. The PMD state was set at 96 ps (average of DGD distribution). The number of CMA taps was chosen to be 101. This large value is designed to increase the resolution of the transfer function of the CMA filters, obtained by Fourier Transform of the impulse responses.

5.1. Impulse responses of the CMA filters

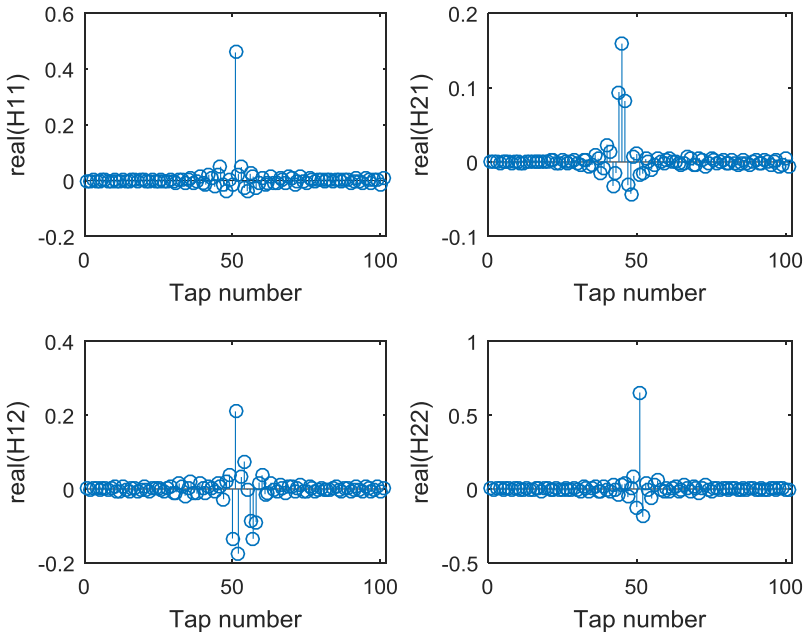

Figure 5-1: Real values of the four complex CMA filters.

In Figure 5-1 and Figure 5-2, we represent the complex-valued impulse responses of the four CMA filters obtained after convergence. For a perfect transmission without any

birefringence, only the central taps of H11 and H22 would have non-zero values, and these values would be real and equal for both filters. In this instance however, from the description of polarization effects made in Section 2.2.5, we can clearly see from CMA values that the polarization had to correct a large amount of birefringence in order to retrieve both tributaries.

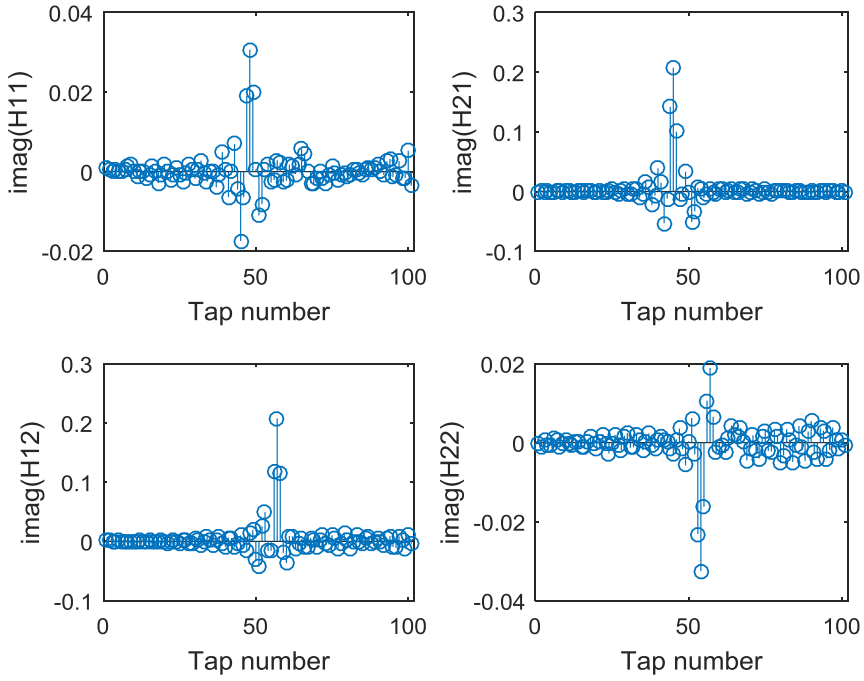

Figure 5-2: Imaginary values of the four complex CMA filters

5.2. Transfer functions of the CMA filters

The method described in [78] to retrieve polarization parameters from the CMA coefficients relies on the frequency dependent transfer functions of the CMA filters, which are obtained by applying a Fourier transform to the impulse responses presented in figures above. These transfer functions are displayed in Figure 5-3 and Figure 5-4.

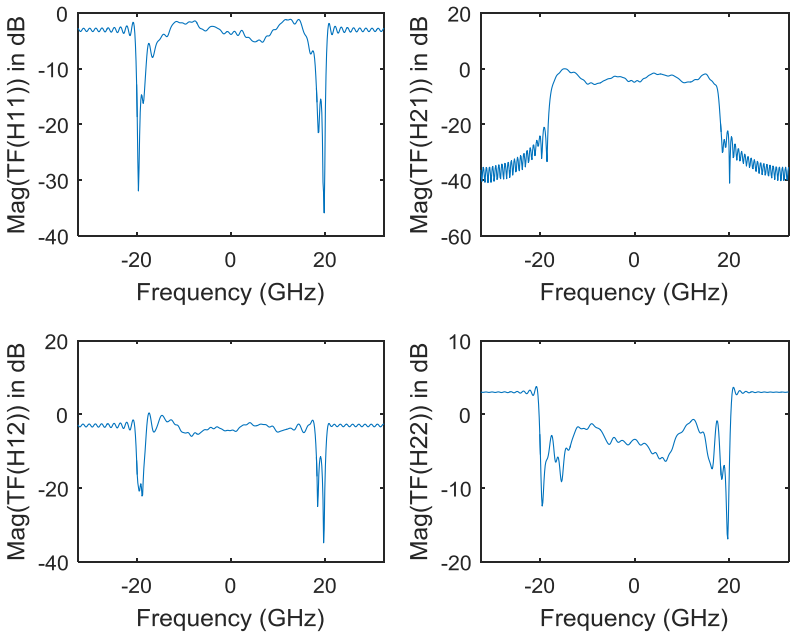

Figure 5-3: Magnitudes in dB of the transfer functions of the CMA filters

On Figure 5-3, we can observe the role of equalizer played by the CMA: a frequency-dependent gain is applied to the input signals so that the spectra of the output signals are as flat as possible for frequencies at least between ±0.5*Baudrate, corresponding to a MMSE equalization. This equalization has an important role to play in the interpretation of polarization parameters measurements. We can also point out what happens in the regions where the signal frequency is close to the Nyquist frequency. The Nyquist frequency is determined has being half of the sampling frequency of the ADC used at receptions right after the photodiodes. In our case, this frequency is close to 20 GHz, determined by the sampling frequency of the real-time oscilloscope used in the experiment.

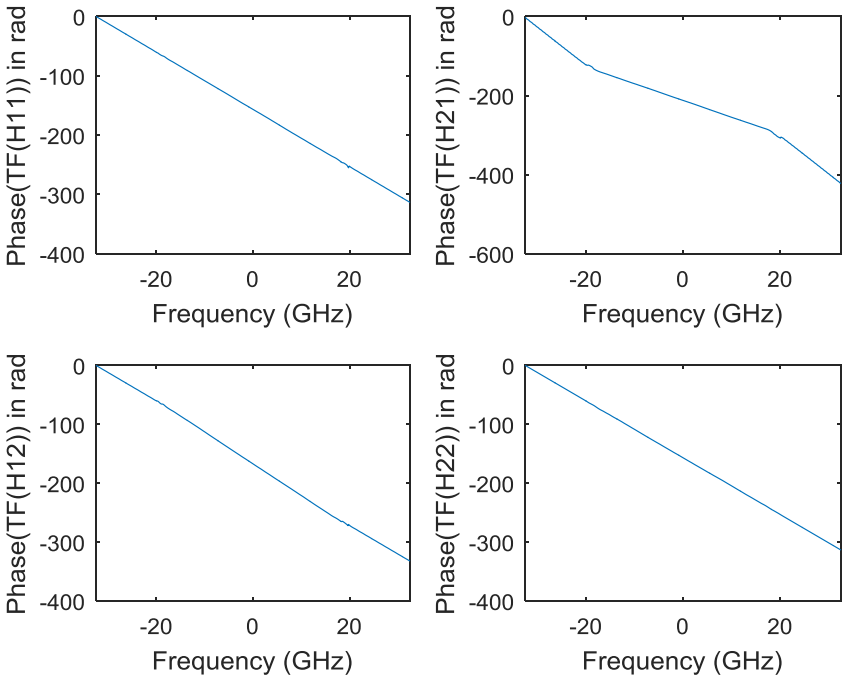

Figure 5-4: Phases in radians of the transfer functions of the CMA filters

The phases applied by the CMA to the input signals are dominantly linear in this case because of the very low chromatic dispersion accumulated in the back-to-back transmissions. The same phases can be used when CD values are not negligible in addition to the CD compensation to correct the residual CD. Such correction of residual CD will take the form of non-negligible second-order term of the phases as functions of the frequency.

5.3. Retrieval of the PDL

In the method described by Hauske et al [78], the PDL of the transmission can be retrieved through the calculation of the frequency-dependent determinant (or cross-product) of the frequency-dependent CMA transfer matrix. Since all PMD and polarization rotation matrices expressed in Jones space have unitary determinants, the determinant of the CMA transfer matrix only contains the product of the determinants of PDL elements along the transmission. In Figure 5-5, we represent the absolute value of the square root of the determinant of the CMA matrix.

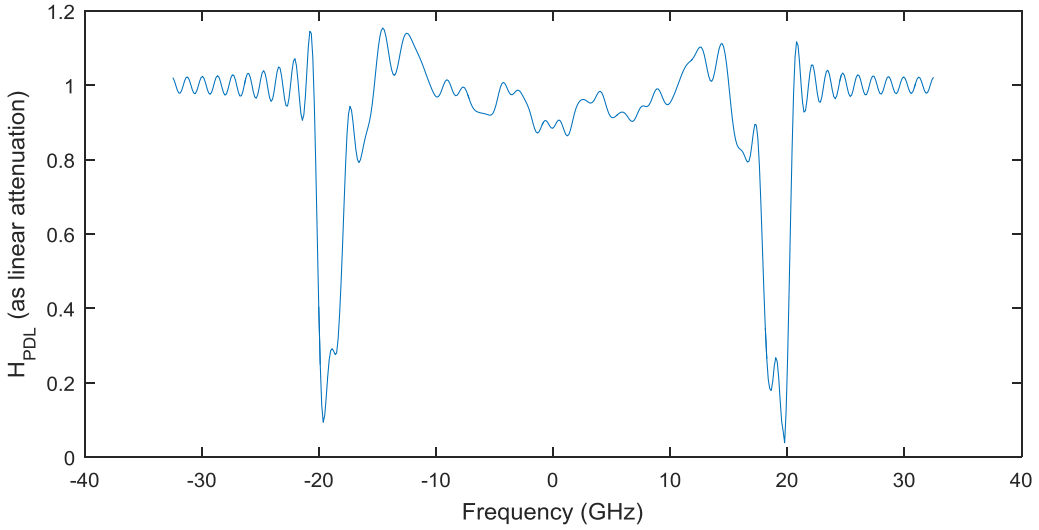

Figure 5-5: H_{PDL} function used by Hauske et al to read PDL value, displayed as an attenuation function of the frequency

It is important to point out here that according to [78], the value of the H_{PDL} function should be superior to unity so that the linear PDL deduced from the measurement is inferior to unity, which is not the case in our experiment. It is due to the fact that the determinant method cannot resolve whether the measured PDL is the actual PDL or the inverse of the PDL. This issue can be solved by sorting which of the two possibilities provides a PDL inferior to 1. Also, because of the equalization, PDL readings will only make sense in frequency regions where the attenuation of the signal from the optical or electrical filters is negligible, usually close to the zero frequency. In our experiment, a PDL of approximately 0.8 is found, which roughly corresponds to 1.9dB. Accuracy of this value is disputable. An inherent difficulty of PDL determination is that the result will depend on the normalization of the RMS values of acquired signals before processing. This normalization is meant to remove the influence of the non-uniformity of the sensitivities of the four photodiodes, and the non-perfect balance of the arms of the coherent mixer. Because of this normalization process, the measured PDL from the proposed method will integrate the imperfections of the receiver, and will not therefore be fully representative of the PDL effect in between the Tx and Rx. Another method is probably necessary to measure the PDL with meaningful accuracy.

5.4. Retrieval of the residual CD

According to Hauske et al, the residual CD can be determined from a polynomial fit of the phase of the square root of the determinant of the CMA matrix. For our back-to-back experiment, the corresponding result is presented in Figure 5-6. In this case, since the accumulated CD is extremely low compared to a regular transmission, the function used for residual CD measurement does not exhibit any second order term. We point out that the back-to-back measurement can be used to assess the minimal detectable residual CD of the algorithmic method, as the minimal amount of residual CD that will result in a measurable (i.e. above noise) second-order term in the displayed function.

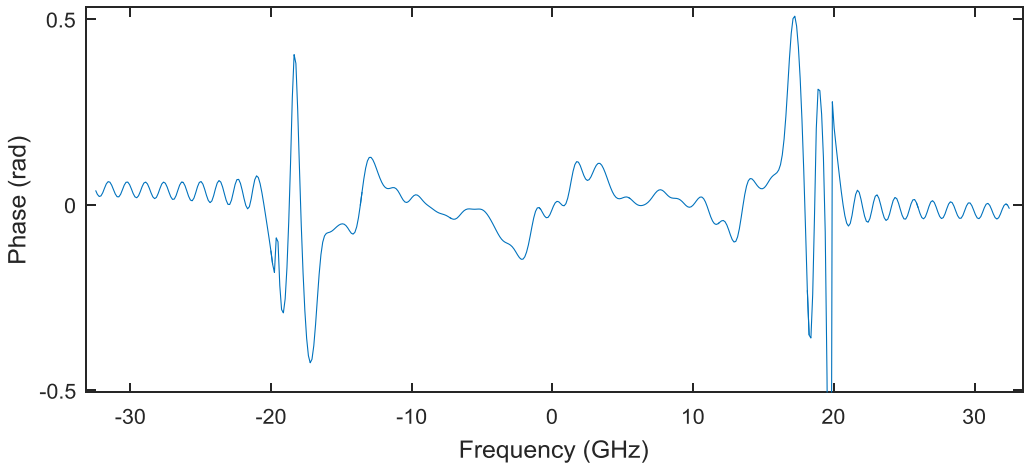

Figure 5-6: Phase of the square root of the determinant of the CMA matrix as a function of the frequency.

5.5. Retrieval of the PMD

The method proposed by Hauske et al to measure the PMD relies on the normalization of the CMA matrix by the square root of its determinant. Then, by numerical differentiation, the derivatives of the components of the normalized CMA matrix in relation to the frequency are calculated. The digital group delay (DGD) corrected by the CMA is then deduced from the determinant of the derived normalized CMA matrix. We point out at here that the measured DGD value only makes sense if it is a positive integer. We check this property by displaying in Figure 5-7 the ratio between the imaginary part and the real part of the calculated DGD for our acquisition.

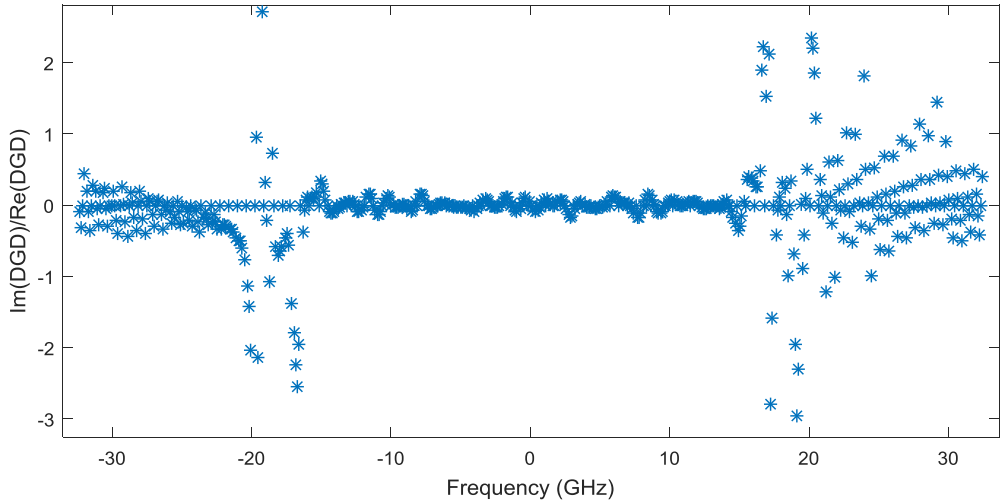

Figure 5-7: Ratio between the imaginary and real parts of the measured DGD

In the central frequency region, we observe from Figure 5-7 that the calculated DGD has, in average, a negligible imaginary part, and thus has physical meaning. However, this is clearly not the case when frequency is, in absolute value, close to the ±0.5*Baudrate and beyond.

In Figure 5-8, we plot the real part of the measured DGD as a function of the frequency. According to the previous part, we expect the values obtained outside the central frequency region to be meaningless. In the central region however, we measure a DGD for our acquisition of approximately 140 ps which is consistent with the set of the deterministic PMD source at 96 ps.

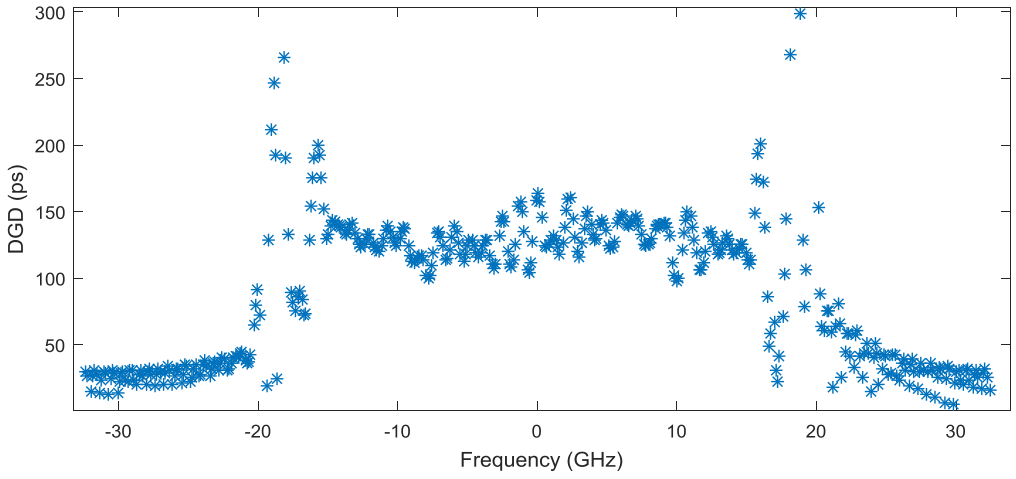

Figure 5-8: Real part of the measured DGD

5.6. Conclusion

A first test of the method of Hauske et al to determine polarization parameters such PDL and PMD shows consistent results for the evaluation of the PMD. However, further experiments need to be performed, specifically to compare the value obtained from the CMA to that obtained with a reference measuring instrument. As for the determination PDL, we point out that the method used here could be inaccurate due to the inherent impossibility to distinguish real PDL effects from imperfections due to the coherent receiver.

6. Monitoring parameters targeted in ORCHESTRA and associated specifications

6.1. Optical Signal to Noise Ratio (OSNR)

OSNR monitoring is one of the most demanded features. The OSNR has traditionally been determined by extrapolating from an out-of-signal-band noise measurement. However, reconfigurable DWDM systems being deployed today require an in-band OSNR measurement. Relation between SNR and OSNR [84]:

$$\frac{1}{SNR} = \frac{1}{SNR_{ASE}} + \frac{1}{SNR_{Tx/Rx}} + \frac{1}{SNR_{NL}},$$

where the SNR_{ASE} is linked to $OSNR_{0.1nm}$ by:

$$\frac{1}{SNR_{ASE}} = \frac{1}{\mu}\frac{1}{\xi OSNR_{0.1\,nm}}.$$

In this equation, μ is the OSNR penalty factor accounting for filtering effect and $\xi = 0.1\ nm$ in $GHz/BaudRate$. Most of the time, this last formula is written by setting μ to 1.

An EDFA cascade could be taken into account by the well admitted relation [85]:

$$OSNR_{OUT} = P_{s,IN} - 10\log_{10}N - NF + 58\ (in\ dB)$$

The formula above works on most situations because most of the variability from one configuration to another is included in the other terms ($SNR_{Tx/Rx}$ and SNR_{NL}). The only alteration to the formula comes from channel distortion, for instance due to optical filtering. Main consequence of distortion is that 1dB OSNR does not exactly translate into 1dB of SNR.

Published measurement approaches (e.g. [86]) proposed on a scheme where non-linear noise is taken into account in OSNR measurements via the calculation of noise correlation between adjacent symbols. One can see also the proposed measurement technique in Polarization Dependent Loss (PDL) part below and especially in the reference [87]. The method from reference [86] seems to provide ONSR estimations over a wide range (specify range) and with an error of ±1 dB. The same accuracy is claimed in [87] but with a zero mean value.

6.2. Polarization Dependent Loss (PDL)

Mainly originating from peculiar components (isolator, WSS, EDFA), we expect margins reductions especially in Metro network where there are more and more nodes. PDL is known to be responsible for performance penalties, and can be hard to mitigate (e.g. over next-gen NxM WSSs [88]).

From [89], the effect of PDL can be modelled as a polarization-dependent OSNR value and directly link to a global Q-factor in some simple but specific cases. Numerous studies [90]–[94] report on PDL and provide the well-established cumulative statistical laws for low-PDL element distributed on link. If all PDL elements share the same value for Γ_{dB}, the PDL coefficient in dB, the probability density function is given by [94]:

$$pdf(\Gamma) = \sqrt{\frac{2}{\pi}} \frac{\Gamma^2 \exp(-\Gamma^2 / (2a^2))}{a^3},$$

where a is related to the number of component and their individual mean value. The mean total value is then given by $\mu = 2a\sqrt{2/\pi}$ and the variance $\sigma^2 = a^2(3\pi - 8)/\pi$.

Nevertheless, impacts of other phenomena on PDL (Non-linear noise, etc.) statistics [95] impose a more general study.

Published PDL measurement schemes [78] report the possibility to extract its value from the equalizer coefficients (CMA) for values above 2dB. The accuracy of this method depends on the OSNR, which is still problematic. To circumvent this issue, authors proposed an alternative scheme [87] which provides access to both PDL and OSNR with very good accuracy mean value and standard deviation within ±1 dB. While the results are relevant, one can note that it is based on “Data-Aided” and (short) “Training Sequence”.

One other proposition is based on a two staged CMA [95] and leads to promising results.

First simulation on proposed measurement technique leads to overestimate the PDL mean value for small PDL value of each component (~0.2 dB). This error is probably

underestimated compared to published results on more complete modelling (e.g. taking into account PMD).

The current implementations considered the quadratic average of PDL elements when the network is designed. Value for each element is taken from statistical measurement on component. We believe that monitoring this criterion will have one of the most meaningful impacts on reducing cost margin.

6.3. Filtering impairments

Filtering impairments are typically due to Wavelength Selective Switches (WSS). Impact of filtering is well-understood in the time domain: it implies a modification of the signal pulses, resulting in Inter-Symbol Interference (ISI). The ISI mitigation at reception (aka equalization) engenders noise amplification. As consequence, a full mitigation of ISI by the equalizer is often suboptimal for overall performance. Thus, final impact of filters comes from a combination of unmitigated ISI, directly due to the distortion, and noise amplification, introduced by the equalization. This makes it particularly challenging to establish a performance model taking into account filtering impairments.

There are several references where the impact of filtering on performance metrics in optical communication networks is simulated and/or measured experimentally [96], [97]. Such effects were specifically discussed in Section 3.

6.4. Channel Power

This parameter is monitored for diagnosis in case of failure and for power setting monitor tool. The Gaussian Noise (GN) model provides a way for setting the power in most systems by optimizing the following equation in a large range of network configuration:

$$SNR = \frac{P}{N_{ASE} + a_{NL} P^3}$$

In the worst case, a precision 1dB on the power will affect the SNR of 1 dB.

There are photodiodes everywhere on optical networks, but there is a real need to aggregate the information between each optical amplifier and improve accuracy at emission and reception. Moreover, this parameter will assess for the overall health state of the optical link (fibre losses, failure and aging). Current design rules are based on value given by the operator concerning the fibre loss, length and type. Moreover, margins are taken to

overcome whole life reparation penalties where monitoring will enable a smoother evolution of the network.

6.5. State of polarization (SOP)

While the monitoring of SOP speed is of paramount importance in pro-active failure detection, a “slow” SOP monitoring would provide useful information on possible outages-appearances of uncorrected blocks (UBs). In this scope, the idea is to perform monitoring of SOP fluctuations over the time to evaluate the amplitude of this variation and assess the risk of outage in case of fast SOP variation. The convergence speed of the CMA is strongly dependent on the SOP of the received waveform, and consequently varies a lot with the choice of the initial finite-impulse response (FIR) filter tap values.

Fast SOP changes can jeopardize proper demultiplexing of the two input polarizations leading to the appearances of the UBs.

The difficult thing about SOP speed measurement is that the DSP sampling rate can be lower than some SOP variations, meaning it can’t be seen with the transponder, whereas UB occurs. If we need to trust a SOP speed monitoring, we need to ensure the sampling rate is much higher than the fast SOP variation. Field measurements of the SOP are used to define the initial number of FIR taps.

References

[1] Y. Pointurier, "Design of low-margin optical networks," Proceedings of the IEEE/OSA Optical Fiber Communication Conference (OFC), Anaheim, CA, USA, 20-24 March 2016, paper Tu3F.5.

[2] J.-L. Augé, "Can we use Flexible Transponders to Reduce Margins?" OFC/NFOEC, Paper OTu2A.1, 2013.

[3] A. Bononi et al., "On the nonlinear threshold versus distance in long-haul highly-dispersive coherent systems", Optics Express (2012).

[4] D. J. Ives, P. Bayvel and S. Savory, "Routing, Modulation, Spectrum and Launch Power Assignment to Maximize the Traffic Throughput of a Nonlinear Optical Mesh Network," Springer Photonic Network Communications, vol. 29, no. 3, pp 244-256 (2015).

[5] L. N. Binh, "Optical Fibre Communications Systems," CRC Press, ISBN: 978-1439806203 (2011).

[6] M. To and P. Neusy, "Unavailability analysis of long-haul networks," IEEE J. Select. Areas Commun., vol. 12, pp. 100–109 (1994).

[7] T. Rahman et al., "On the Mitigation of Optical Filtering Penalties Originating from ROADM Cascade," Photon. Technol. Lett. (2014).

[8] J. Pesic, T. Zami, P. Ramantanis and S. Bigo, "Faster return of investment in WDM networks when elastic transponders dynamically fit ageing of link margins," Proceedings of the IEEE/OSA Optical Fiber Communication Conference (OFC), Anaheim, CA, USA, 20-24 March 2016.

[9] L.E. Nelson et al., "A robust real-time 100G transceiver with soft-decision forward error correction," IEEE J. Opt. Commun. Netw. (2012).

[10] X. Zhou et al., "Rate-Adaptable Optics for Next Generation Long-Haul Transport Networks," IEEE Comm. Mag., vol. 51, no. 3 (2013).

[11] J. Renaudier et al., "Experimental Transmission of Nyquist Pulse Shaped 4-D Coded Modulation using Dual Polarization 16QAM Set-Partitioning Schemes at 28 Gbaud," in Proc. OFC/NFOEC, paper OTu3B.1, (2013).

[12] M.A. Mestre, J.M. Estaran, P. Jennevé, H. Mardoyan and I. Tafur Monroy, "On adaptive transponders for optical slot switched networks: Nyquist-QAM and CO-OFDM experimental comparison," IEEE/OSA J. Lightw. Technol., invited (2016).

[13] A. Bononi, P. Serena, A. Morea and G. Picchi, "Regeneration Savings in Flexible Optical Networks with a New Load-aware Reach Maximization," Elsevier Optical Switching and Networking, in press.

[14] A. Lord, P. Wright and A. Mitra, "Core networks in the flexgrid era," IEEE/OSA J. Lightw. Technol., vol. 33, no. 5, p. 1126 (2015).

[15] Ciena, "Transforming Margin into Capacity with Liquid Spectrum," white paper (2015).

[16] T. Zami et al., "A new method to plan more realistic optical transparent networks," Bell Labs Technical Journal, vol. 14, no. 4, p 213 (2010).

[17]K. Christodoulopoulos el al., "ORCHESTRA – Optical performance monitoring enabling flexible networking," in Proc. ICTON (2015).

[18]Y. Pointurier, M. Coates and M. Rabbat, "Cross-Layer Monitoring in Transparent Optical Networks", IEEE J. Opt. Commun. Netw. (2011).

[19]D. Zibar, "Machine Learning Techniques in Optical Communication," in Proc. ECOC, paper Th.2.6.1 (2015).

[20]N. Sambo, Y. Pointurier, F. Cugini, L. Valcarenghi, P. Castoldi and I. Tomkos, "Lightpath establishment assisted by off-line QoT estimation in transparent optical networks," IEEE J. Opt. Commun. Netw., vol. 2, no. 11, p. 928 (2010).

[21]http://yenista.com/Transmission-Lasers.html

[22]A. Leven et al., "Frequency Estimation in Intradyne Reception," IEEE Phot. Technol. Letters, Vol. 19, No. 6, March 15, 2007

[23]I. Fatadin et al., "Compensation of Frequency Offset for 16-QAM Optical Coherent Systems Using QPSK Partitioning," IEEE Phot. Technol. Letters, Vol. 23, No. 17, Aug. 11, 2011

[24]S. Dris et al., "Phase Entropy-Based Frequency Offset Estimation for Coherent Optical QAM Systems," Proc. OFC 2012, Los Angeles, USA, March 2012

[25]E. Ip and J. Kahn, "Feedforward Carrier Recovery for Coherent Optical Communications," Journal of Lightwave Technology 25, 2675–2692 (2007).

[26]I. Fatadin et al., "Laser Linewidth Tolerance for 16-QAM Coherent Optical Systems Using QPSK Partitioning," IEEE Photonics Technology Letters 22, 631–633 (2010).

[27]N. Argyris et al., "High Performance Carrier Phase Recovery for Coherent Optical QAM," Proc. OFC 2015, Los Angeles, USA, March 2015.

[28]J. Li et al., "Laser-Linewidth-Tolerant Feed-Forward Carrier Phase Estimator With Reduced Complexity for QAM," Journal of Lightwave Technology 29, 2358–2364 (2011).

[29]J. Bromage, "Raman amplification for fibre communications systems," J. Lightwave Technol. 22, 79-93 (2004).

[30]D. Duff, et al., Measurements and simulations of multipath interference for 1.7 Gbit/s lightwave system utilizing single and multifrequency lasers, Proc. OFC, 1989.

[31]C. R. S. Fludger and R. J. Mears, "Electrical measurements of multipath interference in distributed Raman amplifiers," J. Lightwave Technol. 19, 536-545 (2001).

[32]C. H. Kim, J. Bromage, and R. M. Jopson, "Reflection-induced penalty in Raman amplified systems," IEEE Photonics Technol. Lett. 14, 573-575 (2002).

[33]J. Bromage, C. H. Kim, P. J. Winzer, L. E. Nelson, R-J. Essiambre, and R. M. Jopson, "Relative impact of multiple-path interference and amplified spontaneous emission noise on optical receiver performance," in proceedings of Optical Fibre Communication 2002, (Optical Society of America, Washington, D.C., 2002), pp. 119-120.

[34]A. Artamonov, V. Smokovdin, M. Kleshov, S. A. E. Lewis, and S.V. Chernikov, "Enhancement of double Rayleigh scattering by pump intensity noise in fibre Raman amplifiers," in proceedings of Optical Fibre Communication 2002, (Optical Society of America, Washington, D.C., 2002), pp. 186.

[35]C. R. S. Fludger, V. Handerek, and R. J. Mears, "Pump to signal RIN transfer in Raman fibre amplifiers," J. Lightwave Technol. 19, 1140-1148 (2001).

[36]C. H. Kim, "System impairment caused by the combined effect of pump-intensity noise and reflection in Raman amplified system," Electron. Lett. 41, 661-662 (2005).

[37]C. H. Kim, “Analysis of combined effect of pump-intensity noise and reflection in counter-pumped Raman amplifiers”, Optics Express, Vol. 13, No. 16 (2005)

[38]G. P. Agrawal, “Lightwave technology: telecommunication systems”, Wiley, 2005.

[39]M. Zamani, C. Li, Z. Zhang, “Polarization-Time Code and 4 × 4 Equalizer Decoder for Coherent Optical Transmission”, IEEE Photonics Technology Letters, Vol. 24, NO. 20, October 15, 2012

[40]P. Delesques, et al. “Outage probability derivations for PDL-disturbed coherent optical communication”, Signal Processing in Photonic Communications, Optical Society of America, 2012. p. SpTu3A. 5.

[41]P. Delesques, E. Awwad, S. Mumtaz, G. Froc, P. Ciblat, Y. Jaouen, G. Rekaya, C. Ware, “Mitigation of PDL in Coherent Optical Communications: How Close to the Fundamental Limit?”, Proceedings ECOC 2012, P4.13

[42]A. Morea et al., “Throughput Comparison between 50 GHz and 37.5 GHz-grid Transparent Networks [Invited]”, JOCN, Vol. 7, Issue 2, pp. A293-A300 (2015).

[43]M. N. Chughtai, “Study of physical layer impairments in high speed optical networks,” Licentiate Thesis in Communication Systems, KTH School of Information and Communication Technology, Sweden, 2012.

[44]B. Collings, “FlexGrid Technologies,” presented at workshop WS08, ECOC, Amsterdam, Netherlands, September 2012.

[45]I. Mohamed *et al.*, "Analytical Analysis of In-Band Crosstalk, Out-of-Band Crosstalk and GVD-Based Power Penalties in DWDM and TDM/DWDM-PONS", Journal of Computer Science, Volume 11, Issue 3, Pages 573-589.

[46]Z. Dong et al., “Optical Performance Monitoring in DSP-based Coherent Optical Systems”, OFC, 2015. p. W4D. 1.

[47]G. Bosco, A. Carena, R. Cigliutti, V. Curri, P. Poggiolini, F. Forghieri, “Performance prediction for WDM PM-QPSK transmission over uncompensated links”, Proc. of OSA/OFC/NFOEC 2011, paper OTh07

[48]P. Poggiolini et al, “Analytical Modeling of Nonlinear Propagation in Uncompensated Optical Transmission Links”, IEEE Phot. Tech. Letters, vol. 23, no. 11, pp 742 – 744 (2011)

[49]Y. Gao et al., “Intra-channel nonlinearities mitigation in pseudo-linear coherent QPSK transmission systems via nonlinear electrical equalizer,” Opt. Commun., vol. 282, no. 12, pp. 2421–2425, June 2009.

[50]S. Randel et al, “Analysis of RF-Pilot-based phase noise compensation for coherent optical OFDM systems,” IEEE Photon. Technol. Lett., vol. 22, no. 17, pp. 1288–1290, August 2010.

[51]A. Diaz et al, “Analysis of back-propagation and RF pilot-tone based nonlinearity compensation for a 9×224 Gb/s POLMUX 16-QAM system,” OFC 2012.

[52]X. Liu et al, “Phase-conjugated twin waves for communication beyond the Kerr nonlinearity limit,” Nature Photonics, vol. 7, pp. 560–568, 2013.

[53]E. Ip and J.M. Kahn, “Digital Equalization of Chromatic Dispersion and Polarization Mode Dispersion”, Journal of Lightwave Technology, vol. 25, no. 8, August 2007.

[54]A. Carena, V. Curri, G. Bosco, P. Poggiolini, and F. Forghieri,” Modeling of the Impact of Nonlinear Propagation Effects in Uncompensated Optical Coherent Transmission Links”, Journal of Lightwave Technology, Vol. 30, Issue 10, pp. 1524-1539 (2012)

[55]H. Louchet et al, "Comparison of XPM and XpolM-induced impairments in mixed 10G – 100G transmission," Transparent Optical Networks (ICTON), 2011 13th International Conference on , vol., no., pp.1,4, 26-30 June 2011

[56]C. Xie, "Impact of nonlinear and polarization effects on coherent systems," Optical Communication (ECOC), 2011 37th European Conference and Exhibition on , vol., no., pp.1,3, 18-22 Sept. 2011

[57]A. Bononi et al, "Which is the dominant nonlinearity in long-haul PDM-QPSK coherent transmissions?," Optical Communication (ECOC), 2010 36th European Conference and Exhibition on , vol., no., pp.1,3, 19-23 Sept. 2010

[58]P. Jennevé, A. Morea, C. Delezoide, S. Bigo, "Why Pulse shape for cost-sensitive metro networks should differ from optimal pulse shape for long-haul networks", Asia Communications and Photonics Conference (ACP), Hong Kong, Chine, 19-23 November 2015.

[59]Le Nguyen Binh, "Optical Fiber Communications Systems," CRC Press, ISBN: 978-1439806203, June 8, 2011.

[60]M. Schiano et al., "Flexible Node Architectures for Metro Networks," Proc. OFC, W3J.4, Los Angeles (2015).

[61]V. Vusirikala et al., "Scalable and Flexible Transport Networks for Inter-Datacenter Connectivity," Proc. OFC, Tu3H.1, Los Angeles (2015).

[62]Infinera, "ACG Research Market Release, DCI Optical Networking Market", http://www.infinera.com

[63]European FP7 project IDEALIST D1.1

[64]R. A. Shafik et al., "On the Extended Relationships Among EVM, BER and SNR as Performance Metrics," 4th International Conference on Electrical and Computer Engineering ICECE 2006, 19-21 December 2006, Dhaka, Bangladesh

[65]F. Pittalà et al., "Joint PDL and in-band OSNR monitoring supported by data-aided channel estimation", OFC 2012

[66]D. J. Ives et al., "Estimating OSNR of equalised QPSK signals", ECOC 2011.

[67]S. Dris et al., "Blind SNR estimation for QAM constellations based on the signal magnitude statistics", SPIE 2013

[68]C. Zhu et al., "Statistical moments-based OSNR monitoring for coherent optical systems," Optics Express, Vol. 20, No. 16, 30 July 2012

[69]C. Do et al, "Data-aided chromatic dispersion estimation for polarization multiplexed optical systems," IEEE Photonics Journals, Vol. 4, 2037-2049 (2012)

[70]R. A. Soriano et al., "Chromatic dispersion estimation in digital coherent receivers," J. Lightw. Technol., Vol. 29, pp. 1627–1637, (2011)

[71]M. Kuschnerov et al., "Adaptive chromatic dispersion equalization for non-dispersion managed coherent systems," in Proc. OFC 2009, paper OMT1 (2009)

[72]D. Wang et al., "Adaptive chromatic dispersion compensation for coherent communication systems using delay-tap sampling technique", IEEE Photon Technol. Lett., Vol. 23, pp 1016-1018, 2011

[73]C. Malouin et al., “Natural Expression of the Best-Match Search Godard Clock-Tone Algorithm for Blind Chromatic Dispersion Estimation in Digital Coherent Receivers” in Proc. SPPCom. 2012, paper SpTh2B.4

[74]Q. Sui et al., “Fast and robust blind chromatic dispersion estimation using auto-correlation of signal power waveform for digital coherent systems,” J. Lightw. Technol., Vol. 31, pp. 306–312, (2013)

[75]L. Cheng et al, “Chromatic Dispersion Monitoring Based on Variance of Received Optical Power”, Photonics Technology Letters, vol. 23, no. 8, April 2011.

[76]R. Corsini et al., “Blind Adaptive Chromatic Dispersion Compensation and Estimation for DSP-Based Coherent Optical Systems,” J. Lightw. Technol., Vol. 31, np. 13, JULY 1, 2013

[77]X. Yuan et al, “DSP based high precision real-time inline PMD monitoring”, ACP 2010

[78]F. Hauske et al, “Optical Performance Monitoring in Digital Coherent Receivers”, Journal of Lightwave Technology, vol. 27, no. 16, August 2009

[79]F. Hauske and P. J. Stassar, “Novel Trends in Performance Monitoring”, OFC 2012

[80]M. Faruk et al, “Multi-Impairments Monitoring from the Equalizer in a Digital Coherent Optical Receiver”, ECOC 2010

[81]K. P. Ho and J.M. Kahn, “Electronic Compensation Technique to Mitigate Nonlinear Phase Noise," J. Lightwave Technol. 22, 779-783 (2004)”

[82]S. Shen, “Optical performance monitoring for next generation coherent optical communication systems”, Thesis in Electrical Engineering, The Hong Kong Polytechnic University, 2011

[83]J. Renaudier, et al. “Carrier phase estimator for non-linear impairment monitoring and mitigation in coherent optical systems”, US Patent App. 13/513,950, 2012

[84]F. Vacondio, O. Rival, C. Simonneau, E. Grellier, A. Bononi, L. Lorcy, J.-C. Antona, and S. Bigo, “On nonlinear distortions of highly dispersive optical coherent systems,” *Opt. Express*, vol. 20, no. 2, pp. 1022–1032, 2012.

[85]S. Bigo, “Communications optiques haut débit Conception et validation,” *Techniques de l’ingénieur Télécommunications optiques*, vol. TIB454DUO, no. e7081, 2015.

[86]Z. Dong, A. P. T. Lau, and C. Lu, “OSNR monitoring for QPSK and 16-QAM systems in presence of fibre nonlinearities for digital coherent receivers,” *Opt Express*, vol. 20, no. 17, pp. 19520–34, 2012.

[87]F. Pittalà, F. N. Hauske, Y. Ye, N. Guerrero Gonzalez, and I. Tafur Monroy, “Joint PDL and in-band OSNR monitoring supported by data-aided channel estimation,” in *Optical Fibre Communication Conference*, 2012, p. OW4G–2.

[88]P. Giernatowicz, “JDSU TrueFlex Product Roadmap,” 2015.

[89]T. Duthel, C. R. Fludger, J. Geyer, and C. Schulien, “Impact of polarisation dependent loss on coherent POLMUX-NRZ-DQPSK,” in *Optical Fibre Communication Conference*, 2008, p. OThU5.

[90]A. Mecozzi and M. Shtaif, “The statistics of polarization-dependent loss in optical communication systems,” *Photonics Technology Letters, IEEE*, vol. 14, no. 3, pp. 313–315, 2002.

[91]A. Mecozzi and M. Shtaif, "Signal-to-noise-ratio degradation caused by polarization-dependent loss and the effect of dynamic gain equalization," *Journal of lightwave technology*, vol. 22, no. 8, p. 1856, 2004.

[92]L. E. Nelson, C. Antonelli, A. Mecozzi, M. Birk, P. Magill, A. Schex, and L. Rapp, "Statistics of polarization dependent loss in an installed long-haul WDM system.," *Opt Express*, vol. 19, no. 7, pp. 6790–6, 2011.

[93]E. Awwad, "Emerging Space-Time Coding Techniques for Optical Fibre Transmission Systems," 2015.

[94]N. Rossi, P. Serena, and A. Bononi, "Polarization-Dependent Loss Impact on Coherent Optical Systems in Presence of Fibre Nonlinearity," *Photonics Technology Letters, IEEE*, vol. 26, no. 4, pp. 334–337, 2014.

[95]C. Xie and S. Chandrasekhar, "Two-stage constant modulus algorithm equalizer for singularity free operation and optical performance monitoring in optical coherent receiver," in *Optical Fibre Communication Conference*, 2010, p. OMK3.

[96]Y. Sakamaki, T. Kawai, T. Komukai, M. Fukutoku, and T. Kataoka, "Evaluation of optical filtering penalty in digital coherent detection system," *IEICE Communications Express*, vol. 1, no. 2, pp. 54–59, 2012.

[97]A. Ghazisaeidi, P. Tran, P. Brindel, O. Bertran-Pardo, J. Renaudier, G. Charlet, and S. Bigo, "Impact of tight optical filtering on the performance of 28 Gbaud Nyquist-WDM PDM-8QAM over 37.5 GHz grid," in *Optical Fibre Communication Conference*, 2013, p. OTu3B–6.